JCI insight

Position-5-Driven Reorientation of an Immunodominant HLA-A*24:02 SARS-CoV-2 Epitope Drives Universal T-cell Escape

Takeshi Nakama, Aaron Wall, Garry Dolton, Li-Rong Tan, Hannah Thomas, Hiroshi Hamana, Yoshiki Aritsu, Toong Seng Tan, Mako Toyoda, Yoshihiko Goto, Huanyu Li, Mizuki Kitamatsu, Keiko Udaka, Yusuke Miyashita, Hiroyuki Oshiumi, Kimitoshi Nakamura, Yoji Nagasaki, Rumi Minami, Hirotomo Nakata, Pierre J. Rizkallah, Hiroyuki Kishi, Takamasa Ueno, Andrew K. Sewell, Chihiro Motozono

JCI Insight. 2026. https://doi.org/10.1172/jci.insight.202235.

Research In-Press Preview Immunology Infectious disease

Graphical abstract

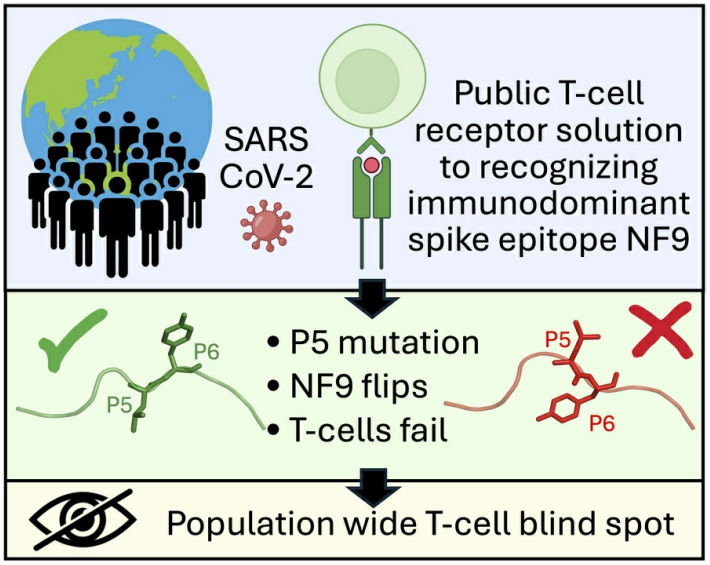

Position-5-Driven Reorientation of an Immunodominant HLA-A*24:02 SARS-CoV-2 Epitope Drives Universal T-cell Escape

Takashi Nakama[1†], Aaron Wall[2†], Garry Dolton[2†], Li-Rong Tan[2], Hannah Thomas[2], Hiroshi Hamana[3], Yoshiki Aritsu[1], Toong Seng Tan[1], Mako Toyoda[1], Yoshihiko Goto[1], Huanyu Li[1], Mizuki Kitamatsu[4], Keiko Udaka[5], Yusuke Miyashita[6, 7], Hiroyuki Oshiumi[6], Kimitoshi Nakamura[7], Yoji Nagasaki[8], Rumi Minami[9], Hirotomo Nakata[10], Pierre J Rizkallah[2], Hiroyuki Kishi[3], Takamasa Ueno[1], Andrew K. Sewell[1,2‡*], Chihiro Motozono[1‡*]

[1] Division of Infection and Immunity, Joint Research Center for Human Retrovirus infection, Kumamoto University, Kumamoto 8600811, Japan
[2] Division of Infection and Immunity, Cardiff University School of Medicine, CF14 4XN Cardiff, Wales, UK
[3] Department of Immunology, Faculty of Medicine, Academic Assembly, University of Toyama, Toyama 9300194, Japan
[4] Department of Applied Chemistry, Faculty of Science and Engineering, Kindai University, Osaka 577-8502, Japan
[5] Department of Immunology, Kochi University, Kochi 7838505, Japan
[6] Department of Immunology, Graduate School of Medical Sciences, Faculty of Life Sciences, Kumamoto University, Kumamoto 8608556, Japan
[7] Department of Pediatrics, Graduate School of Medical Sciences, Kumamoto University, Kumamoto 8608556, Japan
[8] Division of Infectious Diseases, Clinical Research Institute, National Hospitalization Organization, Kyushu Medical Center, Fukuoka 8108563, Japan
[9] Internal Medicine, Clinical Research Institute, National Hospital Organization, Kyushu Medical Center, Fukuoka 8108563, Japan
[10] Department of Hematology, Rheumatology and Infectious Diseases, Kumamoto University School of Medicine, Kumamoto University Hospital, Kumamoto 8608556, Japan

[†] & [‡] Contributed equally

*Correspondence to

Professor Andrew Sewell,
Henry Wellcome Building
University Hospital wales,
Cardiff,
CF14 4XN
UK
SewellAK@cardiff.ac.uk

Professor Chihiro Motozono
Division of Infection and Immunity,
Joint Research Center for Human Retrovirus infection,
Kumamoto University,
2-2-1 Honjo, Chuo-ku, Kumamoto,
860-0811
Japan
motozono@kumamoto-u.ac.jp

AW has move to The University of South Wales Cardiff since completion of this work

Conflict of interest: The authors declare that no competing interests exist.

GRAPHIC ABSTRACT

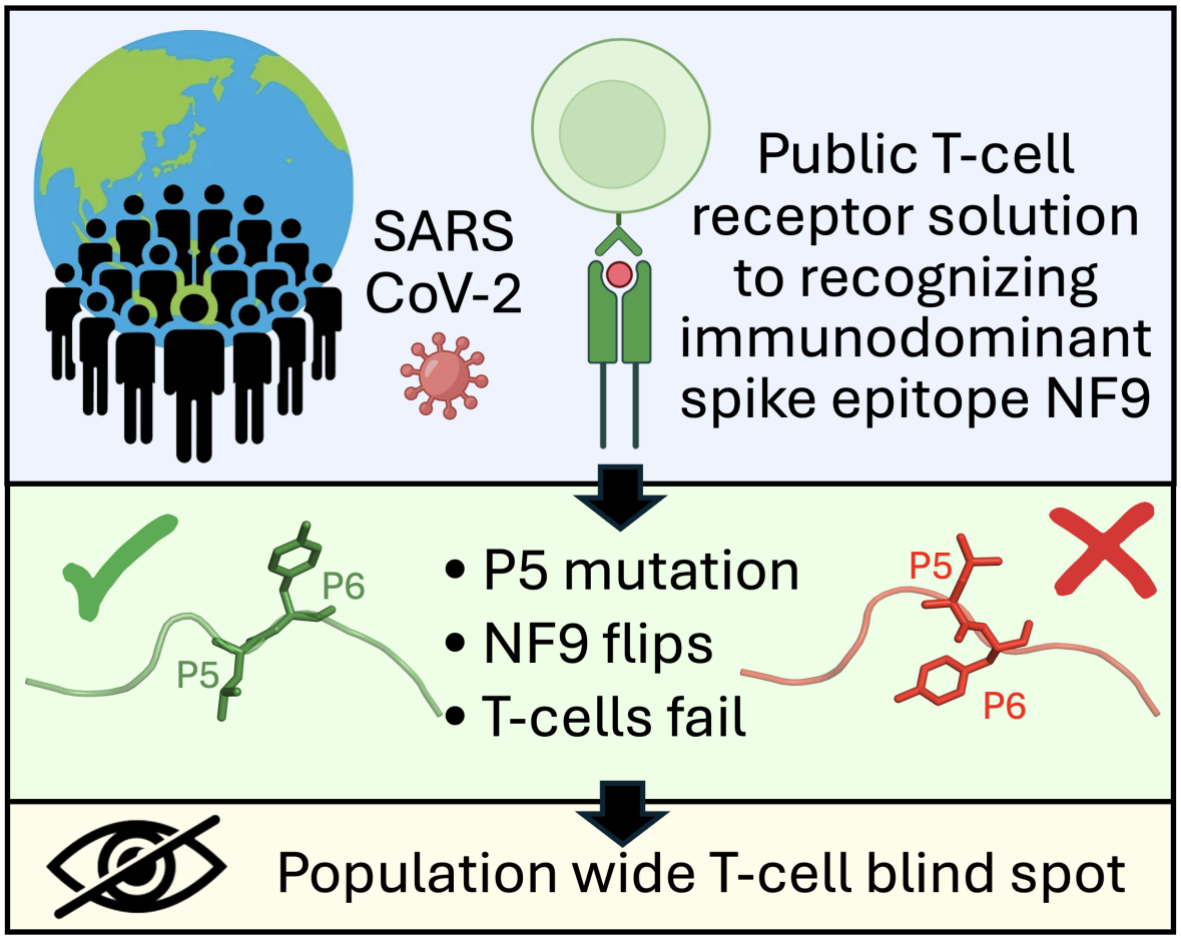

ABSTRACT (200 words)

Cytotoxic T lymphocytes form a critical component of SARS-CoV-2 immunity by recognizing viral peptides bound to HLA class I molecules. Here, we identified the Spike-derived peptide NYNYLYRLF$_{448-456}$ (NF9) as the immunodominant HLA-A*24:02-restricted epitope in both convalescent and vaccinated donors. Across cohorts, A24/NF9-specific responses were dominated by public TCR motifs featuring TRAV12-1 (or TRAV6-1) paired with TRBJ2-7 and a conserved CDR3β sequence (**CASS**XXX**GYEQYF**). Using a panel of thirteen TCRs, we mapped recognition of single amino acid substitutions within NF9 and identified residue 5 (L452) as the principal determinant of escape. The L452R substitution, characteristic of the Delta variant, abolished recognition across all tested TCRs despite preserved HLA binding. Crystallography of a representative public TCR (P1-15) revealed that mutation at position 5 reoriented the peptide within HLA-A*24:02, flipping the adjacent Y453 side chain into the peptide-binding groove and eliminating the dominant TCR contact. This position-5-driven conformational switch provided a structural mechanism for universal loss of NF9 recognition by HLA-A*24:02-restricted T-cells. Consistent with this, Delta-infected convalescents failed to mount *de novo* NF9-5R-specific responses while retaining responses to the conserved A24/QI9 Spike epitope. Together, these findings defined the basis of A24/NF9 recognition and showed how one mutation remodelled peptide presentation to abrogate TCR responses.

INTRODUCTION

Cytotoxic T lymphocytes (CTLs) play a central role in antiviral immunity by detecting and eliminating infected cells that present viral peptides on human leukocyte antigen (HLA) class I molecules. In SARS-CoV-2 infection, CTLs play a pivotal role in immune protection and are associated with reduced disease severity (1, 2). Indeed, individuals can control infection in the absence of detectable antibodies, indicating that cellular immunity alone can confer protection (3-5). Robust CTL responses against conserved coronavirus epitopes are linked to milder COVID-19 (6) and the *HLA-B*15:01* allele has been associated with asymptomatic infection, likely due to pre-existing, cross-reactive T-cells primed by other β-coronaviruses (7).

Given the selective pressure imposed by CTLs, and drawing from experience with chronic viral infections like HIV-1 (8), it was anticipated that SARS-CoV-2 would evolve mutations conferring escape from T-cell recognition as the COVID-19 pandemic progressed (9). Intra-host longitudinal analyses have confirmed that escape from $CD8^+$ T-cells contributes substantially to SARS-CoV-2 evolution (10) and several reports have shown that escape variants can be transmitted and propagated (9, 11, 12). We previously demonstrated that the Spike L452R mutation, which emerged in the Delta variant, enabled escape from HLA-A*24:02-restricted NF9-specific CTLs in both convalescent and vaccinated individuals (13, 14). Likewise, we reported that the P272L mutation in the spike protein that circulated during the second wave of the COVID-19 pandemic escaped from HLA-A*02:01-restricted CTLs elicited by infection or vaccination (9). Escape from T-cell recognition is not confined to $CD8^+$ cells but extends to $CD4^+$ responses (15, 16). While the diversity of HLA alleles across the population makes complete T-cell escape by SARS-CoV-2 improbable (17), dominant responses restricted by common HLAs are expected to leave mutational “footprints” in the viral genome as seen in HIV-1 (18-21). Tracking of the H3N2 influenza virus since the 1968 Hong Kong pandemic indicates that similar immune-driven footprints have resulted in the loss of a predominant CD8 T-cell epitope approximately every three years (22). Understanding how viral mutations subvert T-cell immunity is crucial for vaccine design, predicting variant evolution, and strengthening preparedness for future pandemics.

Against this backdrop, we focused on CTL responses restricted by HLA-A*24:02, a globally prevalent HLA allele enriched in Asian, Oceanian, and Indigenous American populations, and present in ~60% of the Japanese cohort we studied (23). The prominence of *HLA-A*24:02* in regions housing over half of the world's population, makes it a particularly relevant to global resistance to emerging infectious diseases. HLA A*24:02 is of further interest in SARS-CoV-2 infection as it is associated with a decreased risk of severe outcomes (23). Some CTL responses, especially those that target constrained regions of viral proteins, are likely to present more of a challenge for viruses to escape from. Indeed, immunodominant CTL have been linked to control of HIV-1 viremia (8, 24) and public cross-reactive T-cell receptors (TCRs) can mediate such control in an HLA-dependent manner (24-26). Consequently, monitoring of SARS-CoV-2 mutation in the context of dominant T-cell responses offers valuable insight for rational vaccine design and may inform strategies against future emerging pathogens.

Here, we define the molecular basis of immune recognition and escape at the immunodominant HLA-A*24:02-restricted SARS-CoV-2 $Spike_{448-456}$ epitope NYNYLYRLF (NF9). We previously reported that immune escape at this epitope often involves substitution of the leucine at position 5 (P5), suggesting its importance for TCR engagement (13, 14). However, structural and biophysical analyses reveal that the adjacent tyrosine at position 6 (P6) forms the dominant TCR contact, accounting for over a quarter of peptide-TCR interactions. Surprisingly, the P5 L452R mutation induces a conformational rearrangement in A24/NF9 that reorients the P6 tyrosine toward the HLA cleft, rendering it inaccessible to TCRs and thereby enabling population-wide immune escape.

RESULTS

NF9 is the dominant spike epitope in HLA-A*24:02^{+} vaccinees

The *HLA-A*24:02* allele is the most prevalent HLA class I allele in Southeast Asian populations and one of the most widely distributed globally (27). During the COVID-19 pandemic, an inverse correlation was observed between SARS-CoV-2-related deaths per 100,000 population and the prevalence of *HLA-A*24:02*, highlighting the potential protective role of this allele (23). We and others previously identified two immunodominant SARS-CoV-2 spike (S)-derived epitopes presented by HLA-A*24:02: NYNYLYRLF (A24/NF9, residues 448–456) and QYIKWPWYI (A24/QI9, residues 1208–1216) (13, 14, 28, 29). To comprehensively assess the relative immunodominance of these epitopes within the broader spike-specific T-cell response, we screened PBMCs from 11 *HLA-A*24:02*$^{+}$ individuals who had received two doses of BNT162b2 or mRNA-1273. IFN-γ ELISpot assays were performed with overlapping 15-mer peptides (11-amino acid overlap) spanning the entire Spike protein (method as in (30) donor details in **Table S1**) (**Fig. 1A**). To maximize the use of available PBMC, two overlapping peptides (OLPs) were screened per well, allowing coverage of the full Spike sequence with limited cell numbers. Strong *ex vivo* T-cell responses were detected against OLP pairs 111–112 and 301–302, which incorporate the NF9 and QI9 epitopes, respectively. Among all peptide pairs tested, the NF9-containing peptide (OLP112) elicited the most robust (**Fig. 1B**) and frequent (**Fig. 1C**) responses, confirming NF9/A24 as the dominant HLA-A*24:02-restricted spike epitope in mRNA vaccinees. Responses to A24/NF9 were observed in 7 of 11 donors, while A24/QI9 responses were detected in 4 of 11 (**Fig. 1C**), consistent with previous tetramer-based studies (14). To validate this immunodominance, PBMCs from *HLA-A*24:02*$^{+}$ (n = 14) and *HLA-A*24:02*^{neg} (n = 13) vaccinated donors were stimulated with the NF9 peptide and cultured for 14 days. T-cell activation, measured by co-expression of CD25 and CD137 revealed that NF9-specific CD8^{+} T-cells were induced in all *HLA-A*24:02*$^{+}$ individuals (median: 5.15%) but not in *HLA-A*24:02*^{neg} donors (median: 0.30%) (***$p < 0.0001$, **Figure 1D**, **Supplemental Figures S1A&B**), confirming HLA-A*24:02 restriction. Direct *ex vivo* tetramer staining further supported this conclusion. Vaccinated *HLA-A*24:02*$^{+}$ donors had significantly higher frequencies of A24/NF9 tetramer^{+} CD8^{+} T-cells compared to

unvaccinated *HLA-A*24:02*$^{+}$ controls (p = 0.0167, **Figure 1E**, **Supplemental Figures S1C&D**). Moreover, across nine vaccinated HLA-A*24:02^{+} donors, the frequency of A24/NF9 tetramer^{+} cells strongly correlated with the magnitude of NF9-specific CD8^{+} T-cell responses after *in vitro* peptide expansion (R = 0.9006, ***p = 0.0009, **Supplemental Figure S1E**). Together, these data establish A24/NF9 as the dominant spike-derived epitope in HLA-A*24:02^{+} vaccinees and confirm that the response is strictly dependent on HLA-A*24:02 for presentation. Next, we analyzed A24/NF9 and A24/QI9 specific T-cells in both vaccinated and convalescent donors.

The response to HLA-A*24:02 NF9 involves shared TCR features across donors

Single-cell sorting of *ex vivo* PBMCs was performed following NF9/A24 tetramer staining (31) (see **Supplemental Tables S1 and S2**), and the T-cell receptor (TCR) repertoires of A24/NF9 specific T-cells were analyzed for vaccinated (n = 9) and convalescent (n = 4). The TCRα and TCRβ sequences revealed clear convergence in repertoire usage. Most notably, we observed recurrent use of the *TRBJ2-7* gene segment (CDR3 amino acid residues **GYEQYF**) for both vaccinees and convalescent donor (**Figures 2A&B** and **Supplemental Figures S2-4**), which contributed to a highly conserved CDR3β motif in the form **CASS**XXX**GYEQYF**, where "X" represents variable residues (**Figure 2C** and **Supplemental Figures S2-4**). This public CDR3β motif was frequently associated with TRBV2 or TRBV6-1 (contributing CDR3 amino acid residues **CASS**) (**Figure 2B** and **Supplemental Figures S2-4**). For the TCRα chains, the *TRAJ* gene segments usage was highly varied, and for TRAV genes there was a bias towards *TRAV12-1* (**Figures 2A-C** and **Supplemental Figures S2-4**). The CDR3β motif and public TRAV12-1^{+} clonotypes were also detected in A24/NF9-specific CD8^{+} T-cells from other published cohorts (32, 33) (**Supplemental Figure S5**). These data demonstrate that this TCR pattern is consistent across studies and independent of whether T-cells were induced by vaccination or infection, indicating a strong structural selection for TCRs that can productively engage the A24/NF9 complex.

TCR cross-reactivity at position 5 of the HLA A*24:02 NF9 peptide

The L452 residue of the SARS-CoV-2 Spike protein lies within the receptor-binding domain and forms the fifth position (P5) of the A24/NF9 epitope. Mutations at this site, including L452R and L452Q, were characteristic of the Delta, Epsilon, and Lambda variants and later appeared in multiple Omicron-derived lineages such as BA.5, BQ.1 BA.2.86 and JN.1 (34, 35). To define how amino acid substitutions at this position affect immune recognition, we synthesized a panel of NF9/5X peptides (a positional "X-scan" where "X" represents any proteogenic amino acid substitution at P5). All variant peptides bound efficiently to HLA-A*24:02 (**Supplemental Table S3**), consistent with previous report that this position is not a primary HLA anchor (36). We next evaluated TCR recognition using eight representative A24/NF9 TCRs using TRAV12-1 and incorporating the CDR3β motif **CASS**XXX**GYEQYF** (TRBV2 or TRBV6-1, and TRBJ2-7), and additionally five other TCRs with similar features to that of the canonical TCRs (**Figure 3A** and **Supplemental Figure S6** for NF9 tetramer staining). Across all thirteen TCRs the index leucine at P5 was the most potent agonist (**Figures 3B&C**). Fifteen of twenty substitutions abolished activation across the TCRs, including the naturally occurring L452R, L452Q, and L452M mutations (**Figure 3B**). Only isoleucine, threonine, valine, and tryptophan were tolerated, and even these substitutions produced weaker responses (**Figure 3B&C**). Peptide titrations confirmed that NF9-5L from the Wuhan strain was the strongest agonist, while NF9-5R was not recognized by any TCR even at 100 nM peptide (**Figure 3C**). For completeness, we also included the Y453F mutation (NF9-6F) associated with a SARS-CoV-2 outbreak in farmed Mink (37) (**Figure 3C**). These data indicate that TCRs using TRAV12-1, and possessing the CDR3β **CASS**XXX**GYEQYF** motif, and also non-canonical TCRs, have limited capacity to tolerate amino acid substitutions at P5 of the NF9 peptide. These data confirm that the NF9-5L sequence found in the original SARS-CoV-2 'Wuhan' strain and present in COVID-19 vaccines was the strongest agonist for these T-cells. Importantly, none of the NF9-specific T-cell clones, including those with non-canonical TCR pairings, responded to NF9-5R. Together these findings demonstrate that all NF9-specific clonotypes, show a strong preference for the NF9-5L 'Wuhan' sequence. The L452R substitution found in Delta and subsequent variants therefore provides profound, population-wide escape from A24/NF9-

specific T-cell recognition. We next explored this escape further by examining the binding of a canonical TCR to NF9 variants.

Strong P1-15 TCR binding to HLA A*24:02-NF9 but weak or absent binding to all other NF9 variants

To investigate the molecular basis of A24/NF9 recognition and cross-reactivity, we focused on representative public TCR P1-15, isolated from convalescent donor KK-008 (TRAV12-1, TRBV6-1, CDR3β **CASS**SGG**GYEQYF**, and TRBJ2-7). Surface Plasmon Resonance (SPR) was used to quantify equilibrium binding affinities between the P1-15 TCR and HLA-A*24:02 complexes presenting either the wild-type or variant NF9 peptides (**Figure 4A**). Most antiviral TCR-pHLA class I interactions exhibit affinities in the range of K_D = 1-10 μM (38). In contrast the P1-15 TCR bound to A24/NF9 with a KD of 0.67 μM, placing it among the highest affinity natural antiviral TCRs reported to date and suggesting that this interaction is close to the upper limit for naturally occurring A24/NF9-specific TCRs. This unusually strong binding is compatible with, but does not itself define, the convergent public architecture observed among A24/NF9-specific clonotypes.

Despite this high affinity, P1-15 exhibited no detectable binding to A24/NF9-5R and only weaker affinity for NF9-5Q (K_D = 6.8 μM), NF9-5M (K_D = 6.7 μM) and NF9-6F (K_D = 54.4 μM) (**Figure 4B**). These affinities closely mirrored functional responses measured in T-cell activation assays (**Figure 4C**). Deng et al. reported affinities for two similar TRAV12-1/TRBV6-1 NF9-specific TCRs, NYN-I and NYN-II, were 13.6 and 8.6 μM (39), more than ten times weaker than P1-15 yet still within the expected antiviral range. Given its high affinity and robust expression yield, we selected P1-15 for crystallization with A24/NF9 and its variant complexes to define the structural basis for immune escape.

P1-15 TCR recognition is governed by NF9 peptide conformation within HLA-A*24:02

To elucidate the structural basis for P1-15 TCR recognition, we crystallized P1-15 in complex with A24/NF9 and solved the structure at 3.1 Å resolution **(Supplemental Figure S7, Supplemental Table S4).** All structures described in this study have been deposited and

validated in the Protein Data Bank **(**P1-15:HLA-A*24:02-NF9 PDB: 28IL, HLA-A*24:02-NF9-6F PDB: 8RJH, HLA-A*24:02-NF9-5R PDB: 8RJI). Note that the P1-15 TCR β-chain construct contained a short N-terminal extension resulting from the expression system, and the PDB numbering therefore begins from the first residue of this construct. For consistency with the published literature (e.g., PDB: 8YE4), amino acid numbering in this manuscript follows the canonical TCR sequence i.e., -3 relative to the PDB files for the β chain. In the P1-15/A24/NF9 complex residues Tyr4, Tyr6, and Arg7 of the peptide projected upward towards the TCR, whereas Try2 and Phe9 were buried as canonical HLA-A*24:02 anchor residues (**Figure 5A**). Analysis of the molecular contacts between the P1-15 TCR and the NF9 peptide (**Supplemental Table S5**) revealed that the TCR interacted extensively through CDR1α (23% of TCR contacts), CDR3α (37%) and CDR3β (40%) (**Figure 5B**). Tyr4, Tyr6, and Arg7 of the peptide were key contact residues for the CDR3α and CDR3β (**Figures 5C&D**). The CDR3β dominance reflected a conserved Tyr99β residue that contributed 18 van der Waals and one hydrogen bonds P1-15 TCR recognition with NF9-7R and NF9-8L, explaining the recurrent *TRBJ2-7* encoded CDR3β motif (**CASS**XXX**GY^{99}EQYF**) across different donors. The recently published A24/NF9–NYN-I TCR complex (39) (bearing similar TRAV12-1/TRBV6-1 pairing, TRBJ2-7 usage and CDR3β motif) bound NF9 in the same “P5-down, P6-up” configuration and with similar TCR CDR3 loop distribution (**Figures 5E&F**), indicating that public NF9-specific TCRs converge on a shared structural solution.

We next solved the structures of HLA-A*24:02 bound to NF9-6F and NF9-5R at 2.6 Å and 2.3 Å resolution, respectively **(Supplemental Figure S7, Supplemental Table S4)**. Both variant peptides retained a similar overall conformation to wild-type NF9 but showed striking rearrangements at P5 and P6 (**Figures 6A&B**). In the wild-type complex, Leu5 pointed downward into the HLA groove, allowing Tyr6 to project upward and form 11 molecular interactions with P1-15. In contrast, the NF9-6F and NF9-5R peptides rotated residue 5 upward, forcing Tyr6 into the groove where it was buried and unavailable for TCR contact. This “P5-up, P6-down” orientation was consistent across all molecules in the crystallographic unit cell, suggesting it represents a stable alternate conformation favored

by the escape variants. The previously published A24/NF9 structure (PDB 7F4W) contains both conformations within the same unit cell, confirming that “P5-down, P6-up” and “P5-up, P6-down” orientations can coexist in the absence of TCR (**Supplemental Figure S7**). Additionally, modelling an Arginine residue into position 5 of the “P5-down” configuration shows substantial steric hindrance even in the model’s most energetically favorable position **(Figure 6C)**. Together, these observations indicate that the TCR selectively engages the “P5-down, P6-up” configuration, which is disfavored by L452R and related mutations. Contact heatmaps (**Figure 6D**) and schematic interaction maps (**Figure 6E**) reveal a tyrosine-centered binding chemistry: CDR3β Tyr99 and CDR3α tyrosines account for most hydrogen-bond and van der Waals contacts to both peptide and HLA helices. This convergence provides a clear structural explanation for the recurrent C-terminal GY(E/Q)QYF motif across A24/NF9-specific clonotypes. Thus, mutation at position 5 enforces a conformational reorientation of the NF9 peptide that prevents productive TCR engagement. This conformational reorientation provides a clear structural mechanism for the universal loss of A24/NF9 recognition observed across public TCRs. The L452R mutation thereby reconfigures peptide presentation to prevent engagement by the dominant TCR repertoire.

HLA-A*24:02 NF9 5L and 5R peptides are not recognized by T-cells in Delta-infected convalescents

Viral escape mutations can, in some cases, elicit new variant-specific T-cell responses capable of recognizing the altered sequence, as observed in HIV-1 and other rapidly evolving viruses (40). We therefore asked whether individuals infected with the SARS-CoV-2 Delta variant, which harbors the L452R substitution at position 5 of the A24/NF9 epitope, could mount new NF9-5R-specific responses. To test this, we analyzed unvaccinated convalescents known to have been infected with the Delta variant and with no prior history of SARS-CoV-2 exposure, representing likely first antigen encounters (**Supplemental Table S2**). PBMCs were stimulated *in vitro* with either A24/NF9 or A24/NF9-5R peptides, and proliferating $CD8^+$ T-cells were assessed by co-expression of CD25 and CD137. In vaccinated HLA-A*24:02^+ donors, both NF9- and QI9-specific T-cells were readily induced

(*p = 0.0156 and **p = 0.0078, respectively) (**Figure 7A** and **Supplemental Figure S8**). In contrast, PBMCs from HLA-A*24:02^{+} Delta-infected convalescents showed no detectable activation following stimulation with either NF9 or NF9-5R peptides (no significance) but could mount a response to A24/QI9 (*p = 0.0391) (**Figure 7B**). *Ex vivo* tetramer staining confirmed the absence of NF9- or NF9-5R-specific CD8^{+} T-cells in these donors, whereas robust A24/QI9-specific populations were detected (*p = 0.0316 vs A24/NF9-specific ones and *p = 0.0156 vs A24/NF9-5R-specific ones) (**Figure 7C**). Together, these data indicate that the L452R substitution abolishes recognition of the A24/NF9 epitope by pre-existing vaccine- or infection-induced T-cells and simultaneously fails to prime *de novo* variant-specific responses. Consequently, the Delta variant created a population-level T-cell “blind spot” within an otherwise immunodominant region, providing a mechanistic link between structural peptide reorientation and immune escape in HLA-A*24:02^{+} individuals.

DISCUSSION

In this study, we dissected the molecular basis of the immunodominant HLA-A*24:02-restricted T-cell response against SARS-CoV-2 and its failure against emerging variants. By combining population-level analysis of vaccinated and convalescent donors with molecular and structural studies, we demonstrate that a single amino acid substitution at position 5 (L452R) within the spike-derived NF9 epitope reorients the peptide within HLA-A*24:02, disrupting TCR engagement and producing complete functional escape. Our data confirm that NF9 represents the dominant HLA-A*24:02-restricted spike epitope after mRNA vaccination and natural infection. The prevalence of shared, “public” TCR clonotypes across unrelated donors, defined by TRAV12-1 and a conserved CDR3β (**CASS**XXX**GYEQYF**) motif, highlights the strong structural constraints that underlie this immunodominance. Although such convergence is typically associated with robust antiviral protection, it also creates population-wide vulnerability when a single mutation can abrogate recognition across the entire public TCR repertoire. Using TCR functional assays and crystallography, we show that the NF9 peptide adopts a “P5-down, P6-up” orientation within HLA-A*24:02 that allows the P6 tyrosine to form the dominant TCR contact. The L452R substitution at P5 cannot be accommodated in this conformation and instead forces the peptide into an alternative “P5-up, P6-down” orientation, burying Tyr6 within the HLA groove. This conformational switch eliminates the major TCR binding hotspot, providing a direct structural explanation for universal escape from A24/NF9-specific T-cells.

Importantly, Delta-infected convalescents failed to generate new T-cell responses against the variant peptide, indicating that L452R creates a T-cell “blind spot” rather than simply shifting the epitope specificity. This distinguishes T-cell escape in SARS-CoV-2 from that generally observed in HIV-1, where escape can drive secondary variant-specific responses (41, 42). The absence of detectable NF9- or NF9-5R-specific responses in Delta convalescents, despite preservation of other HLA-A*24:02-restricted epitopes such as QI9, demonstrates that mutation at L452 renders this immunodominant site invisible to the HLA-A*24:02-restricted CTL repertoire. It is important to note that loss of an immunodominant CD8 T-cell response is unlikely to equate to complete loss of antiviral immunity at the

individual level. In principle, removal of a dominant epitope could permit the expansion of previously subdominant T-cell responses targeting other viral determinants. However, the A24/NF9 response is exceptional in its magnitude, public TCR architecture, and population prevalence, and we did not observe the emergence of variant-specific or compensatory CD8 T-cell responses in Delta-infected convalescents. Moreover, widespread vaccination has artificially skewed human T-cell immunity toward the Spike protein, further amplifying the dominance of epitopes such as NF9. In this context, escape at NF9 is unlikely to be readily offset by redistribution of immunodominance, and instead may create a genuine population-level blind spot. By contrast, the more recent L452W substitution, which became widespread during successive SARS-CoV-2 waves and remains common in many Omicron-derived lineages, mediates a similar but incomplete attenuation of T-cell recognition. In our dataset, a minority of TCRs displayed weak residual activity toward NF9-5W, whereas none recognized NF9-5R (**Figure 3**). The ability of NF9-5W to evade most NF9-specific TCRs likely conferred a selective advantage, but its spread within those lineages may also reflect other fitness gains acquired within the parent viral lineage. Our demonstration that some TCRs retain low-level reactivity toward NF9-5W indicates that this variant does not represent true “fixation escape” at the population level. Rather, it may represent a form of incomplete immune escape, in which partial preservation of TCR recognition allows sufficient TCR-recognition to avoid strong purifying selection while maintaining overall viral fitness.

Our results extend earlier observations of L452-mediated escape (14, 34, 43, 44) by defining the structural mechanism that underlies this phenomenon across multiple naturally occurring substitutions at P5. Whereas Tian et al. (45) analyzed T-cell reactivity in convalescents infected with BA.2.86 or JN.1, our study combines vaccinated and convalescent cohorts across Wuhan, Alpha, and Delta infection, quantifies the immunodominance of A24/NF9 in human immunity, reconstructs 13 distinct public and private TCRs, and resolves the peptide-HLA rearrangement responsible for universal TCR escape. Our work therefore establishes a mechanistic explanation for the widespread loss of recognition observed in later variants.

Together, these data illustrate a unifying principle: mutations at P5 of A24/NF9 act through conformational reorientation rather than simple disruption of direct contacts. Moreover, the emergence and persistence of L452 substitutions support the broader concept that $CD8^+$ T-cell pressure can drive viral evolution at immunodominant epitopes once population immunity is established. This process was first documented for HLA-A*02:01-restricted responses in SARS-CoV-2 (9) and the spread of L452 mutations at the dominant A24-restricted epitope now provides parallel evidence in a distinct HLA context. Together, these examples demonstrate that $CD8^+$ T-cell immunity leaves discernible and predictable signatures on the SARS-CoV-2 genome, consistent with patterns previously observed in HIV-1 and influenza (18-22).

The concept that a single “side-chain flip” can destroy a major antiviral response has broad implications for T-cell immunology. Although similar conformational “molecular switches” have been described for immunodominant epitopes HIV-1 (46) and melanoma antigens (47), the A24/NF9 system provides the clearest example of this mechanism driving population-level escape in a globally circulating human pathogen. Given the high prevalence of HLA-A*24:02, particularly across East and Southeast Asia, structural flipping at this epitope offers a compelling explanation for the rapid expansion of variants carrying substitutions at residue 452. Understanding how peptide structural constraints shape T-cell vulnerability will be critical for the rational design of next-generation vaccines. In summary, we show that position-5-driven reorientation of the immunodominant A24/NF9 epitope underlies universal loss of recognition by public TCRs. This mechanistic insight provides a framework for anticipating viral evolution at structurally constrained epitopes and for prioritizing epitopes that are less amenable to conformational escape as the basis for broadly protective T-cell vaccines.

MATERIALS AND METHODS

Sex as a biological variable.

Sex was not considered as a biological variable in this study.

Collection of human PBMCs

PBMCs were obtained from 28 HLA-A*24:02$^+$ donors vaccinated with BNT162b2- or mRNA-1273 (mean age: 38.0, range: 22-67, 71.4% male), 17 HLA-A*24:02-negative BNT162b2-vaccinated donors (mean age: 34.0, range: 23-57, 70.6 % male), 3 HLA-A*24:02$^+$ unvaccinated donors (mean age: 39.0, range: 22-56, 100 % male), 12 HLA-A24-positive convalescents (mean age: 38.0, range: 23-61, 50.0 % male) and 9 HLA-A24-negative convalescents (mean age: 47.0, range: 33-71, 77.8 % male). PBMCs were isolated by a density gradient centrifugation using Ficoll-Paque Plus (GE Healthcare Life Sciences, Cat# 17-1440-03) and cryopreserved until further use.

Cell Culture

A549 cells stably expressing human ACE2 and HLA-A*24:02-IRES-GFP (generated previously (14)) were maintained in Ham's-F12 (Wako, Cat# 080-08565) supplemented with 10% FBS. C1R cells expressing HLA-A*24:02 (C1R-A2402) were cultured in RPMI 1640 medium (Thermo Fisher Scientific, Cat# 11875101) containing 10% FBS.

ELISpot assay

Ex vivo IFN-γ ELISpot assay was performed using anti-human IFN-γ mAbs 1-D1K (Mabtech, Code:3420-3-1000) and 7-B6-1 (biotinylated detection Mabtech, Code: 3420-6-250) followed by Streptavidin-ALP (Mabtech, Code:3310-8-1000) and AP Conjugated Substrate Kit (BIO-RAD, Cat# 1706432) MultiScreen 96-well plates were prewashed with PBS and blocked with RPMI 1640 medium (Thermo Fisher Scientific, Cat# 11875101) containing 10% FBS. Defrosted PBMCs (1×10^5 per well) were stimulated with overlapping peptides (11 aa overlap) spanning the SARS-CoV-2 Spike protein (2 μg/ml) for 20 h. Spots were counted using ImmunoSpot (Cellular Technology Limited). Positive responses were defined as >3 spots when the negative control showed 0, or >2× the negative control when background spots were present.

Tetramer staining

NF9, NF9-5R, or QI9 and NF9-5R peptide-HLA-A*24:02 tetramers (PE or BV421) were generated using QuickSwitchTM Quant HLA-A*24:02 Tetramer Kit (MBL International Cat# TB-7302-K1 or TB-7302-K4). PBMCs were stained with tetramers for 30 min at room temperature, followed by surface staining with antibodies to: CD8 (APCcy7 HIT8a, 1/100 dilution; Biolegend), CD14 (PerCP/Cy5.5, HCD14, 1/100 dilution; Biolegend), CD3 (AF532,

UCHT1, 1/25 dilution; eBioscience), CD19 (SB436, HIB19, 1/50 dilution; eBioscience). Dead cells were excludedusing 7-aminoactinomycin D (Biolegend, Cat# 420404). Fixed samples (1% paraformaldehyde, Nacalai Tesque, Cat# 09154-85), were acquired on a FACS Canto II (BD Biosciences) or Cytek Northern Lights (Cytek, Japan) and analysed using FlowJo v10 software.

Activation Induced Marker Assay

Activation induced marker assay was performed as previously described (13, 14, 43). Briefly, PBMCs were pulsed with 100 nM NF9, NF9-5R or QI9 peptides (Scrum Inc.) and cultured for 10-14 days. in RPMI 1640 medium with 10% FBS and 30 U/mL IL-2 (PeproTech). Expanded $CD8^+$ T-cells were restimulated with or without the peptide for 24 h at 37°C and stained with antibodies to CD3 (FITC, UCHT1, 1/100 dilution), CD8 (APCcy7, RPA-T8, 1/100 dilution), CD14 (PerCP/Cy5.5, HCD14, 1/100 dilution), CD19 (PerCP, Cy5.5 HIB19, 1/100 dilution), CD25 (PEcy7, M-A251, 1/50 dilution) and CD137 (APC, 4B4-1, 1/50 dilution; Biolegend). Samples were analyzed by flow cytometry as above.

The peptide-dependent stabilization assay

Performed as described (48). TAP-deficient C1R-A24 cells were incubated at 26°C overnight. with 1 μM β2-microglobulin (β2m) and graded peptide concentrations in 96-well U-bottom plates. Cells were stained with FITC-labeled Bw4-specific mAb 17A12 (provided by Dr. Ulrich Hämmerling) and analyzed by FACScan (BD, San Jose, CA, USA). Binding was normalized using high-binder peptide (TYLPTNASL) and low-binder peptide (RVWESATPL) controls.

TCR cDNA amplification from single T-cells and construction of TCR expression vector

A24/$NF9^+$ or A24/QI9/$A24^+CD8^+$7-AAD^- T-cells were single-cell sorted into 96-well plates. TCRα and TCRβ cDNA were amplified using one-step multiplex RT-PCR (31) and sequenced. Clonotypes were analyzed with IMGT/V-QUEST. Assembled TCRβ-P2A-TCRα-P2A-BlaR fragments were cloned into the PiggyBac vector (SBI, Cat# PB530A-2) by the Gibson assembly method.

TCR sensitivity assay

PB TCR-P2A-BlaR was electroporated into JurkatΔ-Luc with transposase (SBI, Cat# PB200PA-1) using Neon® (Thermo Fisher Scientific 1200v, 5 ms, 5 pulses). Transfectants were selected with 10 μg/ml of blasticidin-S for 10-14 days. TCR-expressing Jurkat cells were cocultured with A549-ACE2-A2402 cells (E:T ratio of 2:1) for 6 h. Luciferase activity

was measured using Steady-Glo® (Promega, Cat#E2510) on a CentroXS3 plate reader (Berthold Technologies).

Protein expression and purification

Soluble P1-15 TCR protein and biotinylated pMHCI were manufactured as previously described (49). Briefly, codon-optimized P1-15 TCR α and β chains, HLA -A*24:02 heavy chain, and β2m chain gene fragments were generated by GeneArt. All sequences were confirmed by automated DNA sequencing (Eurofins). P1-15 TCR expression constructs were designed with a disulfide-linked construct to produce the soluble domains (variable and constant) for both the α (residues 1–204) and β chains (residues 1–245) (49). The HLA-A*24:02 heavy chain (residues 1–248) (α1, α2, and α3 domains), tagged or not tagged with a biotinylation sequence, and β2m (residues 1–100) were also cloned and used to make the pMHCI complexes. The P1-15 TCR α and β chains, the HLA-A*24:02 heavy chain, and β2m sequences were inserted into separate pGMT7 expression plasmids under the control of the T7 promoter (50). Competent Rosetta DE3 E. coli cells were used to produce the P1-15 TCR α and β chains, HLA-A*24:02 heavy chain and B2m in the form of inclusion bodies (IBs) using 0.5 mM IPTG to induce expression and protein were chemically refolded as described previously (51).

Surface plasmon resonance experiments

TCR:pMHC binding kinetics was determined by SPR as described (52). SPR experiments were conducted using a BIAcore T200 (Cytiva). Biotinylated pMHC molecules were immobilized onto a CM5 sensor chip (Cytiva). HLA-A*24:02-AYAQKIFKIL was bound to flow cell 1 as a negative control, with samples bound to flow cells 2-4. Equilibrium binding analysis was performed at 25°C. Ten serial dilutions of the TCR were made, and 100 mL of each dilution was injected onto the chip. Data was analyzed using GraphPad Prism and fitted to a global fit algorithm. KD values were calculated assuming 1:1 binding using a non-linear fit curve (y= [P1 x]/[P2 + x]).

Crystallization, diffraction data collection, and model refinement

TCR and pMHC protein crystals were grown at 18°C by sitting drop vapor diffusion. TCR or peptide-MHC at a concentration of 10 mg mL-1in a buffer of 10 mM Tris and 10 mM sodium chloride buffer, was dispensed in 200 nL drops into 3 well low profile Intelliplates (Art Robbins Instruments) using the Gryphon liquid handling robot (Art Robbins Instruments). Potential crystallization conditions were created by supplementing the protein with 200 nL from a 96-well crystallization screen and loading the reservoir with 60 mL of the same condition. For the crystallization of TCR:pMHC complexes, both components were mixed in a 1:1 molar ratio and followed the same process as described above. The MIDAS screen (Molecular Dimensions) (10.1107/S0907444910009005) and the T-cell optimized crystal

screen were used for this study (10.1016/j.jim.2012.06.007) with the conditions for each structure reported in the relevant statistics tables (**Table S4**).

Crystals were sent to the Diamond Light Source synchrotron in Oxfordshire, UK. X-ray datasets were collected using a PILATUS 9M pixel detector at a wavelength of 0.98 A˚ and consisted of 3600 images, with 0.1° oscillation and 0.1 s exposure at the I04 MX beamline at the Diamond Light Source. Datasets were processed using the DIALS and AIMLESS pipelines. The CCP4 version 8 software suit (Collaborative Computational Project No. 4) was used to derive 3D models from the reflection intensities (10.1107/S0907444910045749). Phaser version 2.7 was used to conduct molecular replacement (53), Win-Coot version 0.9.6 was used to match the model to the electron density map and add relevant solvents to the 3D structure (10.1107/S0907444904019158), and REFMAC version 5.8 was used to refine the 3D structures (54). 3D protein structures were analyzed, and images were prepared using Pymol version 2.3.4 (Schrodinger, LLC). The reflection data and final coordinates were deposited in the PDB database www.rcsb.org (P1-15:HLA- A*24:02-NF9 PDB: 28IL, HLA-A*24:02-NF9-6F PDB: 8RJH, HLA-A*24:02-NF9-5R PDB: 8RJI).

Statistics

Data were analyzed using GraphPad Prism 10 (Software) or R. Statistical tests are detailed in the figure legends. All experiments were independently replicated at least twice unless otherwise stated.

Data availability

All data supporting the findings of this study are available within the manuscript and its supplemental information. Supporting data values for all figures are provided in the accompanying Excel file. TCR sequences identified in this study are reported in the manuscript and supplemental tables. Additional data are available from the corresponding authors upon reasonable request.

Study approval

All protocols involving human subjects at Kumamoto University and Kyushu Medical Center and Kyushu University were reviewed and approved by the Institutional Review Kumamoto University (approval numbers 461 and 477). Written informed consent was obtained from all participants.

Author Contributions

TN AW GD LRT HT HH YA TS TMT YG HL KU PJR and CM performed the experiments.
YM HO KN YN RM and HN collected clinical samples.
MK HK and TU prepared reagents.
AW and PJR performed crystal structure analysis.
AKS and CM designed the experiments and interpreted the results.
CM wrote the original manuscript.
All authors reviewed and proofread the manuscript.

Funding support

This study was supported in part by AMED Research Program on Emerging and Re-emerging Infectious Diseases (20fk0108539h0001 and 20fk0108451s0101 to T.U.), the AMED Research Program on HIV/AIDS (21fk0410046 to C.M.) and AMED Research Program on Interdisciplinary Cutting-edge Research (23wm0325064 to C.M.). AKS is a Wellcome Investigator (220295/Z/20/Z) and this support funded all work at Cardiff University. Additional support was provided by JSPS KAKENHI Grant-in-Aid for Scientific Research (B) (19H03703, 22H03119 to T.U.) and (22H02877 to C.M.), Fostering Joint International Research (A) (22KK0277 to C.M.), Scientific Research (C) (22K07089 to M.T.). We also acknowledge support from the Takeda Science Foundation (to C.M. and M.T), the intramural grant from Kumamoto University COVID-19 Research Projects (AMABIE) (to C.M.), the IMAI Memorial Trust for AIDS Research (to M.T.) and Shin-Nihon Foundation of Advanced Medical Research (to M.T.).

REFERENCES

1. Rydyznski Moderbacher C, Ramirez SI, Dan JM, Grifoni A, Hastie KM, Weiskopf D, et al. Antigen-Specific Adaptive Immunity to SARS-CoV-2 in Acute COVID-19 and Associations with Age and Disease Severity. *Cell.* 2020;183(4):996-1012 e19.

2. Tan AT, Linster M, Tan CW, Le Bert N, Chia WN, Kunasegaran K, et al. Early induction of functional SARS-CoV-2-specific T cells associates with rapid viral clearance and mild disease in COVID-19 patients. *Cell reports.* 2021;34(6):108728.

3. Le Bert N, Clapham HE, Tan AT, Chia WN, Tham CYL, Lim JM, et al. Highly functional virus-specific cellular immune response in asymptomatic SARS-CoV-2 infection. *J Exp Med.* 2021;218(5).

4. Sekine T, Perez-Potti A, Rivera-Ballesteros O, Stralin K, Gorin JB, Olsson A, et al. Robust T Cell Immunity in Convalescent Individuals with Asymptomatic or Mild COVID-19. *Cell.* 2020;183(1):158-68 e14.

5. Reynolds CJ, Swadling L, Gibbons JM, Pade C, Jensen MP, Diniz MO, et al. Discordant neutralizing antibody and T cell responses in asymptomatic and mild SARS-CoV-2 infection. *Sci Immunol.* 2020;5(54).

6. Mallajosyula V, Ganjavi C, Chakraborty S, McSween AM, Pavlovitch-Bedzyk AJ, Wilhelmy J, et al. CD8(+) T cells specific for conserved coronavirus epitopes correlate with milder disease in COVID-19 patients. *Sci Immunol.* 2021;6(61).

7. Augusto DG, Murdolo LD, Chatzileontiadou DSM, Sabatino JJ, Jr., Yusufali T, Peyser ND, et al. A common allele of HLA is associated with asymptomatic SARS-CoV-2 infection. *Nature.* 2023;620(7972):128-36.

8. Kawashima Y, Pfafferott K, Frater J, Matthews P, Payne R, Addo M, et al. Adaptation of HIV-1 to human leukocyte antigen class I. *Nature.* 2009;458(7238):641-5.

9. Dolton G, Rius C, Hasan MS, Wall A, Szomolay B, Behiry E, et al. Emergence of immune escape at dominant SARS-CoV-2 killer T cell epitope. *Cell.* 2022;185(16):2936-51 e19.

10. Stanevich OV, Alekseeva EI, Sergeeva M, Fadeev AV, Komissarova KS, Ivanova AA, et al. SARS-CoV-2 escape from cytotoxic T cells during long-term COVID-19. *Nature communications.* 2023;14(1):149.

11. Agerer B, Koblischke M, Gudipati V, Montano-Gutierrez LF, Smyth M, Popa A, et al. SARS-CoV-2 mutations in MHC-I-restricted epitopes evade CD8(+) T cell responses. *Sci Immunol.* 2021;6(57).

12. de Silva TI, Liu G, Lindsey BB, Dong D, Moore SC, Hsu NS, et al. The impact of viral mutations on recognition by SARS-CoV-2 specific T cells. *iScience.* 2021;24(11):103353.

13. Motozono C, Toyoda M, Zahradnik J, Saito A, Nasser H, Tan TS, et al. SARS-CoV-2 spike L452R variant evades cellular immunity and increases infectivity. *Cell Host Microbe.* 2021;29:1124-36.

14. Motozono C, Toyoda M, Tan TS, Hamana H, Goto Y, Aritsu Y, et al. The SARS-CoV-2 Omicron BA.1 spike G446S mutation potentiates antiviral T-cell recognition. *Nature communications.* 2022;13(1):5440.

15. Tye EXC, Jinks E, Haigh TA, Kaul B, Patel P, Parry HM, et al. Mutations in SARS-CoV-2 spike protein impair epitope-specific CD4(+) T cell recognition. *Nat Immunol.* 2022;23(12):1726-34.

16. Chen Y, Mason GH, Scourfield DO, Greenshields-Watson A, Haigh TA, Sewell AK, et al. Structural definition of HLA class II-presented SARS-CoV-2 epitopes reveals a mechanism to escape pre-existing CD4(+) T cell immunity. *Cell Rep.* 2023;42(8):112827.

17. Bertoletti A, Le Bert N, and Tan AT. SARS-CoV-2-specific T cells in the changing landscape of the COVID-19 pandemic. *Immunity.* 2022;55(10):1764-78.

18. Matthews PC, Leslie AJ, Katzourakis A, Crawford H, Payne R, Prendergast A, et al. HLA footprints on human immunodeficiency virus type 1 are associated with interclade polymorphisms and intraclade phylogenetic clustering. *J Virol.* 2009;83(9):4605-15.

19. Sun W, Gao C, Hartana CA, Osborn MR, Einkauf KB, Lian X, et al. Phenotypic signatures of immune selection in HIV-1 reservoir cells. *Nature.* 2023;614(7947):309-17.

20. Moore CB, John M, James IR, Christiansen FT, Witt CS, and Mallal SA. Evidence of HIV-1 adaptation to HLA-restricted immune responses at a population level. *Science.* 2002;296(5572):1439-43.

21. Carlson JM, Le AQ, Shahid A, and Brumme ZL. HIV-1 adaptation to HLA: a window into virus-host immune interactions. *Trends Microbiol.* 2015;23(4):212-24.

22. Woolthuis RG, van Dorp CH, Kesmir C, de Boer RJ, and van Boven M. Long-term adaptation of the influenza A virus by escaping cytotoxic T-cell recognition. *Scientific reports.* 2016;6:33334.

23. Fujii SI, Yamasaki S, Iyoda T, and Shimizu K. Association of cellular immunity with severity of COVID-19 from the perspective of antigen-specific memory T cell responses and cross-reactivity. *Inflamm Regen.* 2022;42(1):50.

24. Chen H, Ndhlovu ZM, Liu D, Porter LC, Fang JW, Darko S, et al. TCR clonotypes modulate the protective effect of HLA class I molecules in HIV-1 infection. *Nat Immunol.* 2012;13(7):691-700.

25. Motozono C, Kuse N, Sun X, Rizkallah PJ, Fuller A, Oka S, et al. Molecular basis of a dominant T cell response to an HIV reverse transcriptase 8-mer epitope presented by the protective allele HLA-B*51:01. *J Immunol.* 2014;192(7):3428-34.

26. Price DA, Asher TE, Wilson NA, Nason MC, Brenchley JM, Metzler IS, et al. Public clonotype usage identifies protective Gag-specific CD8+ T cell responses in SIV infection. *J Exp Med.* 2009;206(4):923-36.

27. Gonzalez-Galarza FF, McCabe A, Santos E, Jones J, Takeshita L, Ortega-Rivera ND, et al. Allele frequency net database (AFND) 2020 update: gold-standard data classification, open access genotype data and new query tools. *Nucleic Acids Res.* 2020;48(D1):D783-D8.

28. Kuse N, Zhang Y, Chikata T, Nguyen HT, Oka S, Gatanaga H, et al. Long-term memory CD8(+) T cells specific for SARS-CoV-2 in individuals who received the BNT162b2 mRNA vaccine. *Nature communications.* 2022;13(1):5251.

29. Shimizu K, Iyoda T, Sanpei A, Nakazato H, Okada M, Ueda S, et al. Identification of TCR repertoires in functionally competent cytotoxic T cells cross-reactive to SARS-CoV-2. *Commun Biol.* 2021;4(1):1365.

30. Dang TTT, Anzurez A, Nakayama-Hosoya K, Miki S, Yamashita K, de Souza M, et al. Breadth and Durability of SARS-CoV-2-Specific T Cell Responses following Long-Term Recovery from COVID-19. *Microbiol Spectr.* 2023;11(4):e0214323.

31. Hamana H, Shitaoka K, Kishi H, Ozawa T, and Muraguchi A. A novel, rapid and efficient method of cloning functional antigen-specific T-cell receptors from single human and mouse T-cells. *Biochem Biophys Res Commun.* 2016;474(4):709-14.

32. Rowntree LC, Petersen J, Juno JA, Chaurasia P, Wragg K, Koutsakos M, et al. SARS-CoV-2-specific CD8(+) T-cell responses and TCR signatures in the context of a prominent HLA-A*24:02 allomorph. *Immunol Cell Biol.* 2021;99(9):990-1000.

33. Minervina AA, Pogorelyy MV, Kirk AM, Crawford JC, Allen EK, Chou CH, et al. SARS-CoV-2 antigen exposure history shapes phenotypes and specificity of memory CD8(+) T cells. *Nat Immunol.* 2022;23(5):781-90.

34. Tan TS, Toyoda M, Ode H, Barabona G, Hamana H, Kitamatsu M, et al. Dissecting Naturally Arising Amino Acid Substitutions at Position L452 of SARS-CoV-2 Spike. *J Virol.* 2022;96(20):e0116222.

35. Uriu K, Ito J, Kosugi Y, Tanaka YL, Mugita Y, Guo Z, et al. Transmissibility, infectivity, and immune evasion of the SARS-CoV-2 BA.2.86 variant. *Lancet Infect Dis.* 2023;23(11):e460-e1.

36. Sidney J, Southwood S, and Sette A. Classification of A1- and A24-supertype molecules by analysis of their MHC-peptide binding repertoires. *Immunogenetics.* 2005;57(6):393-408.

37. Koopmans M. SARS-CoV-2 and the human-animal interface: outbreaks on mink farms. *Lancet Infect Dis.* 2021;21(1):18-9.

38. Cole DK, Pumphrey NJ, Boulter JM, Sami M, Bell JI, Gostick E, et al. Human TCR-binding affinity is governed by MHC class restriction. *J Immunol.* 2007;178(9):5727-34.

39. Deng S, Xu Z, Wang M, Hu J, Liu Z, Zhu F, et al. Structural insights into immune escape at killer T cell epitope by SARS-CoV-2 Spike Y453F variants. *J Biol Chem.* 2024:107563.

40. Goulder PJ, and Watkins DI. HIV and SIV CTL escape: implications for vaccine design. *Nat Rev Immunol.* 2004;4(8):630-40.

41. Allen TM, Yu XG, Kalife ET, Reyor LL, Lichterfeld M, John M, et al. De novo generation of escape variant-specific CD8+ T-cell responses following cytotoxic T-lymphocyte escape in chronic human immunodeficiency virus type 1 infection. *J Virol.* 2005;79(20):12952-60.

42. Sun X, Shi Y, Akahoshi T, Fujiwara M, Gatanaga H, Schonbach C, et al. Effects of a Single Escape Mutation on T Cell and HIV-1 Co-adaptation. *Cell reports.* 2016;15(10):2279-91.

43. Kimura I, Kosugi Y, Wu J, Zahradnik J, Yamasoba D, Butlertanaka EP, et al. The SARS-CoV-2 Lambda variant exhibits enhanced infectivity and immune resistance. *Cell reports.* 2022;38(2):110218.

44. Motozono C, Toyoda M, Zahradnik J, Saito A, Nasser H, Tan TS, et al. SARS-CoV-2 spike L452R variant evades cellular immunity and increases infectivity. *Cell Host Microbe.* 2021;29(7):1124-36 e11.

45. Tian J, Shang B, Zhang J, Guo Y, Li M, Hu Y, et al. T cell immune evasion by SARS-CoV-2 JN.1 escapees targeting two cytotoxic T cell epitope hotspots. *Nat Immunol.* 2025;26(2):265-78.

46. Kloverpris HN, Cole DK, Fuller A, Carlson J, Beck K, Schauenburg AJ, et al. A molecular switch in immunodominant HIV-1-specific CD8 T-cell epitopes shapes differential HLA-restricted escape. *Retrovirology.* 2015;12:20.

47. Bianchi V, Bulek A, Fuller A, Lloyd A, Attaf M, Rizkallah PJ, et al. A Molecular Switch Abrogates Glycoprotein 100 (gp100) T-cell Receptor (TCR) Targeting of a Human Melanoma Antigen. *J Biol Chem.* 2016;291(17):8951-9.

48. Mashiba T, Udaka K, Hirachi Y, Hiasa Y, Miyakawa T, Satta Y, et al. Identification of CTL epitopes in hepatitis C virus by a genome-wide computational scanning and a rational design of peptide vaccine. *Immunogenetics.* 2007;59(3):197-209.

49. Laugel B, Boulter JM, Lissin N, Vuidepot A, Li Y, Gostick E, et al. Design of soluble recombinant T cell receptors for antigen targeting and T cell inhibition. *J Biol Chem.* 2005;280(3):1882-92.

50. Garboczi DN, Ghosh P, Utz U, Fan QR, Biddison WE, and Wiley DC. Structure of the complex between human T-cell receptor, viral peptide and HLA-A2. *Nature.* 1996;384(6605):134-41.

51. Cole DK, Dunn SM, Sami M, Boulter JM, Jakobsen BK, and Sewell AK. T cell receptor engagement of peptide-major histocompatibility complex class I does not modify CD8 binding. *Mol Immunol.* 2008;45(9):2700-9.

52. Whalley T, Dolton G, Brown PE, Wall A, Wooldridge L, van den Berg H, et al. GPU-Accelerated Discovery of Pathogen-Derived Molecular Mimics of a T-Cell Insulin Epitope. *Frontiers in immunology.* 2020;11:296.

53. McCoy AJ, Grosse-Kunstleve RW, Adams PD, Winn MD, Storoni LC, and Read RJ. Phaser crystallographic software. *Journal of applied crystallography.* 2007;40(Pt 4):658-74.

54. Murshudov GN, Skubak P, Lebedev AA, Pannu NS, Steiner RA, Nicholls RA, et al. REFMAC5 for the refinement of macromolecular crystal structures. *Acta Crystallogr D Biol Crystallogr.* 2011;67(Pt 4):355-67.

Figure legends

Figure 1. Immunodominant NF9/A24-specific T-cell responses in vaccinated donors.
A. Scaled schematic of SARS-CoV-2 spike the S1 and S2 subunits, signal peptide (SP), receptor binding domain (RBD) and transmembrane domain (TM). Overlapping peptides spanning the Spike peptide used for functional assays. **B**. Magnitude of T-cell responses, and (**C**) fraction of HLA-A*24:02$^+$ donors responding to overlapping peptide (OLP) pairs spanning SARS-CoV-2 S protein (n = 11) as measured by IFN-γ ELISpot. Each well contained two overlapping peptides (11-aa overlap). Positive responses were defined as >3 spot-forming cells above background. OLP pairs 111-112 and 301-302, which encompasses the A24/NF9 and the A24/QI9 epitopes, respectively, are indicated in red and blue with color-matched arrows. **D**. CD25$^+$CD137$^+$CD8$^+$ T-cells from HLA-A*24:02$^+$ and HLA-A*24:02-negative donors following 14-day incubation ± NF9 peptide. Summary data from all donors (n = 14) (****p < 0.0001 by Mann-Whitney test ± NF9 peptide is indicated) Gating strategy is shown in **Fig. S1A**. **E**. Detection of A24/NF9-specific T-cells in PBMCs using A24/NF9 tetramers in vaccinated and unvaccinated HLA-A*24:02$^+$ donors (*p = 0.0167, Mann-Whitney test).). Representative plots are shown in **Fig. S1B**.

Figure 2. T-cell receptor analysis of NF9/A24 and QI9/A24-specific T-cells.
A. TRAV–TRAJ and TRBV–TRBJ gene usage among NF9-specific T-cells from nine vaccinated and four convalescent HLA-A*24:02$^+$ donors. Circos plots depict relative usage of TRAJ/TRBJ (left arcs) and TRAV/TRBV (right arcs), with arc size reflecting gene frequency. Ribbons indicate V–J pairings. **B**. Combined Circos plots from all 13 donors (vaccinated + convalescent) showing TCRα and TCRβ chain usage. A strong bias towards TRAV12-1 and TRBJ2-7 is evident in the α- and β-chains, respectively. **C.** Sequence logo plots showing CDR3α (left) and CDR3β (right) motifs derived from the combined donor set. CDR3α: TRAV12-1$^+$ sequences, most common length = 15 aa. CDR3β: TRBJ2-7$^+$ sequences, most common length = 13 aa. Colored bars at the center indicate the diversity of TRAJ (α-chain) and TRBV (β-chain) gene usage contributing to each motif, ordered by frequency. See **Fig. S2, S3 and S4** for additional TCRα/β characteristics, including full CDR3 length distributions.

Figure 3. Preference for leucine and non-recognition of arginine at P5 by NF9-specific TCRs
A. Paired TCRs from vaccinated or convalescent HLA-A*24:02$^+$ donors that recognize the NYNYLYRLF$_{488\text{-}456}$ Spike peptide. Each TCR's variable (V) and joining (J) segments and corresponding CDR3 sequences are shown. V and J segments are color-coded to match the Circos plots used elsewhere in the study. Black text in CDR3 sequence indicates amino acids derived from P or N nucleotide additions or, for TRB chains, from diversity (D) segments. TRAV12-1 expression and the conserved CDR3β motif CASSXXXGYEQYF (red

star) identify canonical NF9-specific TCRs, with other clonotypes included for comparison. **B.** Heatmap summarizing Jurkat reporter cell activation for each TCR in (A) against single amino acid substitutions at position 5 of the NF9 peptide. Responses are normalized to each TCR's maximal activation to enable parallel comparison. **C.** Titration assays of each TCR from (A) expressed in Jurkat cells, tested against the position 5 variants recognized in (B), as well as the 5R (L452R) escape mutant and the 6F (Y453F) variant identified in farmed mink (37).

Figure 4. Binding affinity and cross-reactivity of P1-15:A24/NF9 interaction.
A. Surface Plasmon resonance (SPR) analysis of P1-15 TCR binding to HLA-A*24:02 complexes presenting NF9 (magenta), NF9-6F (orange), NF9-5R (green), NF9-5Q (red) and NF9-5M (blue). **B**. SPR responses to ten serial dilutions of P1-15 TCR were measured. K_Ds were determined by non-linear fit curve (y= [P1 x]/[P2 + x]). **C.** NFAT-luciferase reporter activity in Jurkat cells transduced with P1-15 TCR and stimulated with NF9 or variant peptides (NF9-5R, NF9-6F, NF9-5Q, and NF9-5M), demonstrating functional sensitivity corresponding to the measured binding affinities.

Figure 5. Structural analysis of the public P1-15 TCR/NF9-A24 complex
A. Presentation of the NF9 peptide (magenta sticks) when in complex with the P1-15 TCR. **B.** Top-down view of the NF9 peptide (white sticks) showing the distribution of the P1-15 CDR loops (blue cartoon). The crossing angle is indicated by the blue line. **C-D** Detailed views of contacts between CDR1α (C), CDR3β (D) and CDR3α and the NF9 peptide (magenta sticks) showing Van der Waals (black dotted lines) and hydrogen (red dotted lines) interactions. **E**. Structural comparison of the NF9 peptide (sticks) bound to P1-15 TCR (magenta) or NYN-I TCR (cyan). **F.** Top-down comparison of the P1-15 (blue cartoon) and NYN-I (cyan cartoon) CDR loop distributions over the NF9 peptide (white sticks).

Figure 6. Structural basis for position-5-driven reorientation of the NF9 peptide within HLA-A*24:02. A. A24/NF9 peptide (magenta sticks) in complex with the P1-15 TCR, with uncomplexed A24/NF9-6F (orange sticks) and A24/NF9-5R (green sticks) structures superimposed, demonstrating side-chain flipping at positions 5 and 6. **B**. Diagram illustrating the alternative "P5-up" (top, green) and "P5-down" (bottom, red) peptide orientations adopted within the peptide–HLA complexes in **A**. **C**. Modelling of the NF9 peptide residue 5 (white sticks) mutated to arginine using PyMOL. Red discs indicate steric clashes; the displayed rotamer produced the fewest clashes after PyMOL energy minimization. **D.** Structural heatmap showing the number and distribution of atomic contacts between each of the P1-15 and NYN-I TCRs and the NF9 peptide. These bonds are also shown in **E,** a schematic representation of intermolecular contacts between NF9 peptide residues and the P1-15 (top) or NYN-I (bottom) TCRs, showing how CDR3 tyrosines dominate the molecular

804 contacts with both HLA and peptide. In **D** blue = no peptide and red = highest contacts with
805 the colors reflecting P1-15 binds much stronger than NYN-1 ($K_D \approx 0.67$ μM vs > 10 μM)
806
807 **Figure 7. NF9-5R-specific T-cells are not detectable in SARS-CoV-2 Delta-infected**
808 **convalescents. A**. Activation-induced marker assay of PBMCs from vaccinated donors with
809 no evidence of prior SARS-CoV-2 infection. Cells were stimulated for 14 days with A24/NF9
810 (NYNYLYRLF448–456) or A24/QI9 (QYIKWPWYI1208–1216) peptides. Data show the
811 percentage of $CD25^+CD137^+$ $CD8^+$ T-cells in HLA-A*24:02-negative (n = 4) and HLA-
812 $A*24:02^+$ (n = 8) donors. Wilcoxon matched-pairs signed-rank test (*p = 0.0156, **p =
813 0.0078). **B**. Activation-induced marker assay of PBMCs from unvaccinated convalescents
814 infected with the SARS-CoV-2 Delta variant. Cells were stimulated with A24/NF9, A24/NF9-
815 5R, or A24/QI9 peptides. Data show the percentage of $CD25^+CD137^+$ $CD8^+$ T-cells in HLA-
816 A*24:02-negative (n = 9) and $A*24:02^+$ (n = 8) donors. Wilcoxon matched-pairs signed-rank
817 test (*p = 0.0391). C. *Ex vivo* detection of HLA-A*24:02-restricted $tetramer^+$ $CD8^+$ T-cells in
818 Delta-infected convalescents. PBMCs from HLA-A*24:02-negative (n = 6) and $A*24:02^+$ (n
819 = 7) donors were stained with tetramers specific for HIV-KW9 (negative control), A24/NF9,
820 A24/NF9-5R, or A24/QI9. Wilcoxon matched-pairs signed-rank test (*p = 0.0156 vs A24/HIV-
821 KW9 and A24/NF9-5R and *p = 0.0312 vs A24/NF9).
822

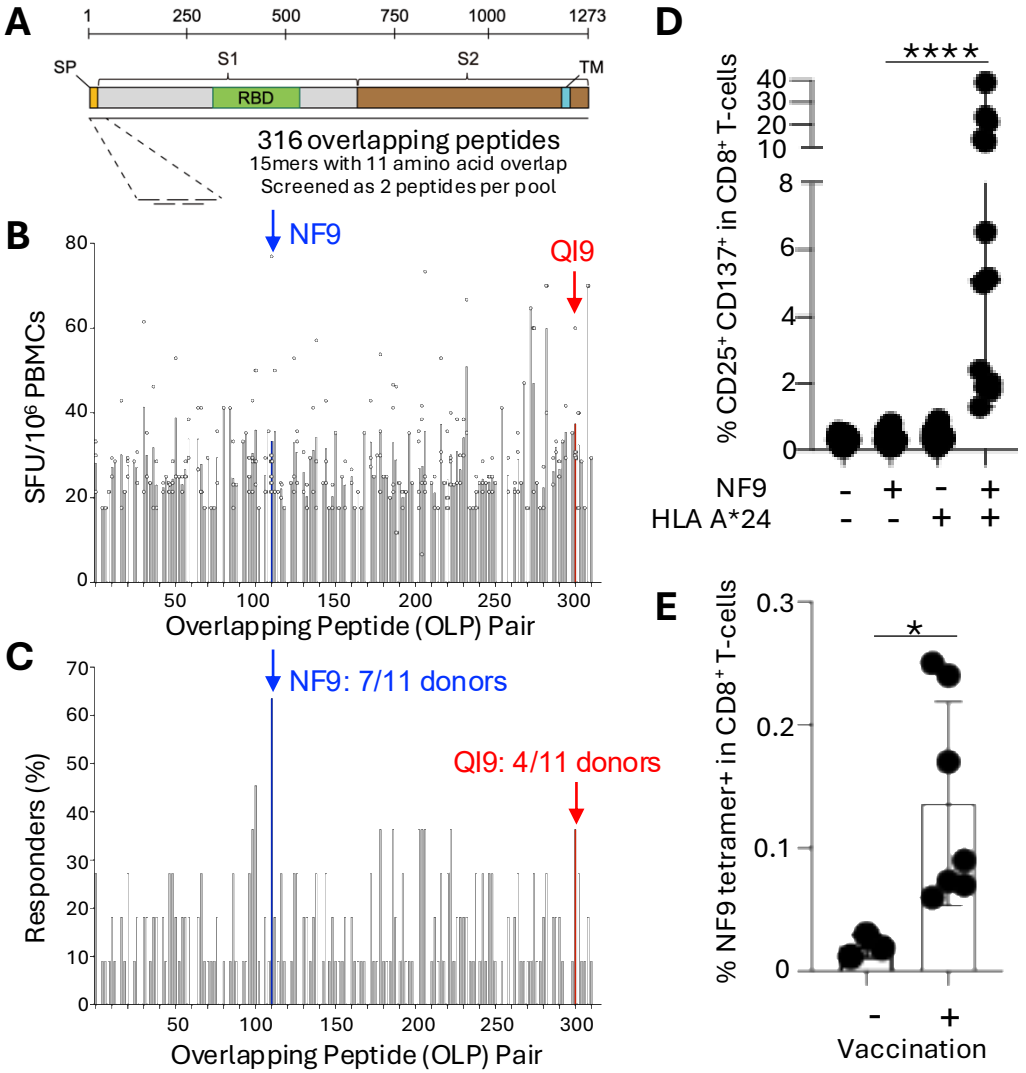

Figure 1. Immunodominant NF9/A24-specific T-cell responses in vaccinated donors.
A. Scaled schematic of SARS-CoV-2 spike the S1 and S2 subunits, signal peptide (SP), receptor binding domain (RBD) and transmembrane domain (TM). Overlapping peptides spanning the Spike peptide used for functional assays. **B**. Magnitude of T-cell responses, and (**C**) fraction of HLA-A*24:02⁺ donors responding to overlapping peptide (OLP) pairs spanning SARS-CoV-2 S protein (n = 11) as measured by IFN-γ ELISpot. Each well contained two overlapping peptides (11-aa overlap). Positive responses were defined as >3 spot-forming cells above background. OLP pairs 111-112 and 301-302, which encompasses the A24/NF9 and the A24/QI9 epitopes, respectively, are indicated in red and blue with color-matched arrows. **D**. CD25⁺CD137⁺CD8⁺ T-cells from HLA-A*24:02⁺ and HLA-A*24:02-negative donors following 14-day incubation ± NF9 peptide. Summary data from all donors (n = 14) (****p < 0.0001 by Mann-Whitney test ± NF9 peptide is indicated) Gating strategy is shown in **Fig. S1A**. **E**. Detection of A24/NF9-specific T-cells in PBMCs using A24/NF9 tetramers in vaccinated and unvaccinated HLA-A*24:02⁺ donors (*p = 0.0167, Mann-Whitney test).). Representative plots are shown in **Fig. S1B**.

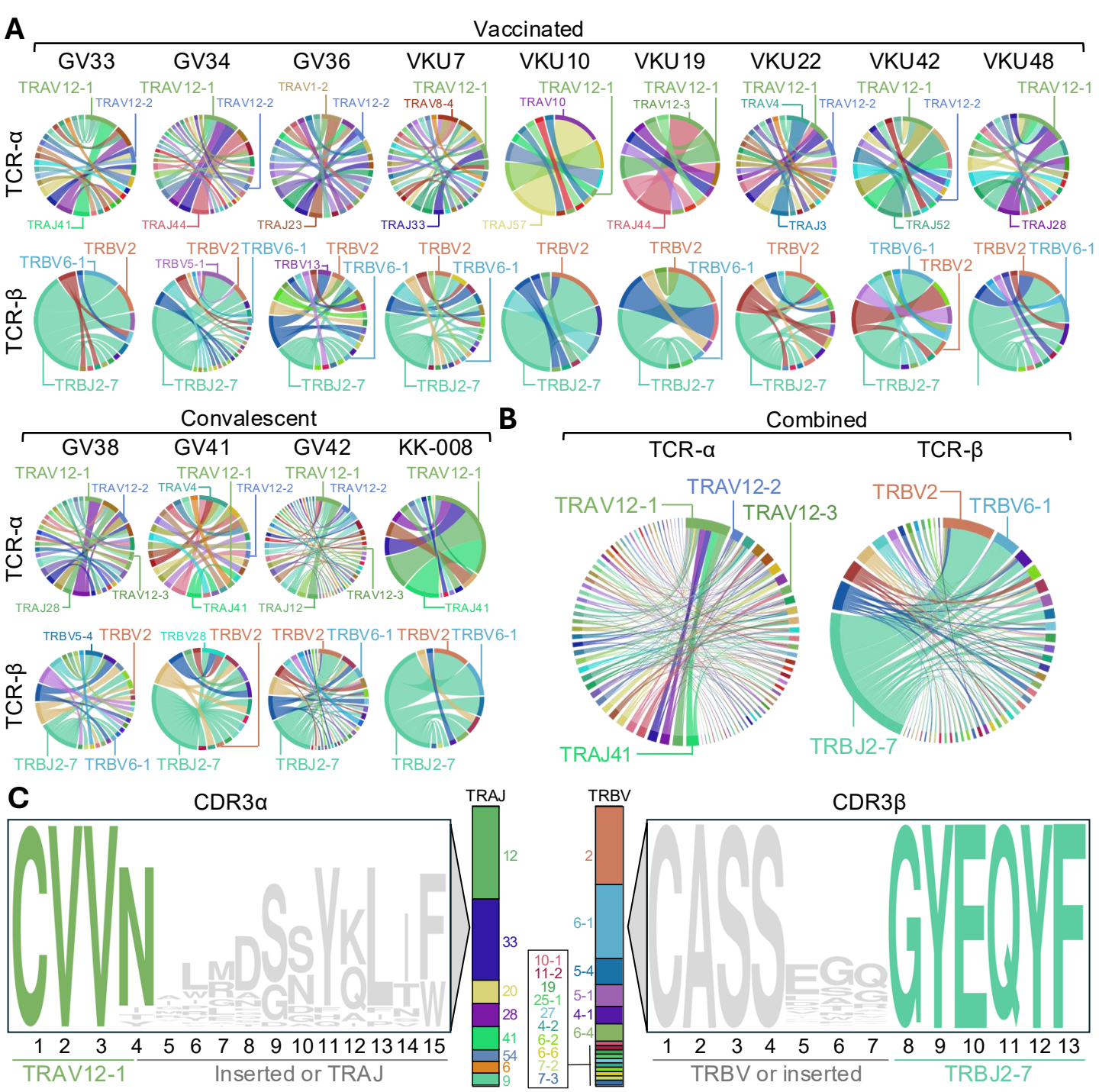

Figure 2. T-cell receptor analysis of NF9/A24 and QI9/A24-specific T-cells.
A. *TRAV–TRAJ* and *TRBV–TRBJ* gene usage among NF9-specific T-cells from nine vaccinated and four convalescent HLA-A*24:02⁺ donors. Circos plots depict relative usage of *TRAJ/TRBJ* (left arcs) and *TRAV/TRBV* (right arcs), with arc size reflecting gene frequency. Ribbons indicate V–J pairings. **B**. Combined Circos plots from all 13 donors (vaccinated + convalescent) showing TCRα and TCRβ chain usage. A strong bias towards TRAV12-1 and TRBJ2-7 is evident in the α- and β-chains, respectively. **C.** Sequence logo plots showing CDR3α (left) and CDR3β (right) motifs derived from the combined donor set. CDR3α: TRAV12-1⁺ sequences, most common length = 15 aa. CDR3β: TRBJ2-7⁺ sequences, most common length = 13 aa. Colored bars at the center indicate the diversity of *TRAJ* (α-chain) and *TRBV* (β-chain) gene usage contributing to each motif, ordered by frequency. See **Fig. S3 and S4** for additional TCRα/β characteristics, including full CDR3 length distributions.

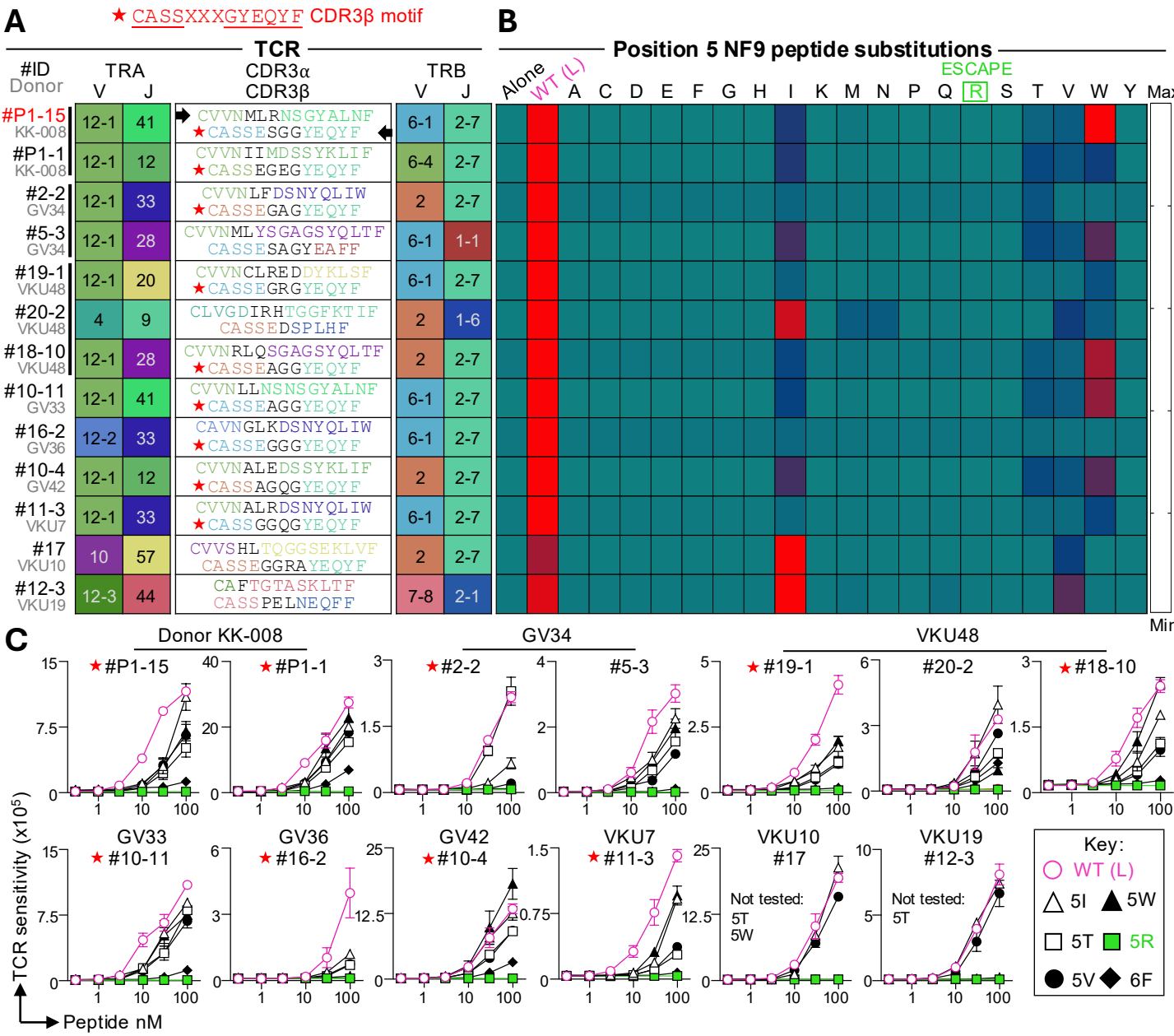

Figure 3. Preference for leucine and non-recognition of arginine at P5 by NF9-specific TCRs

A. Paired TCRs from vaccinated or convalescent HLA-A*24:02^{+} donors that recognise the NYNYLYRLF$_{488\text{-}456}$ Spike peptide. Each TCR's variable (V) and joining (J) segments and corresponding CDR3 sequences are shown. V and J segments are colour-coded to match the Circos plots used elsewhere in the study. Black text in CDR3 sequence indicates amino acids derived from P or N nucleotide additions or, for TRB chains, from diversity (D) segments. TRAV12-1 expression and the conserved CDR3β motif CASSXXXGYEQYF (red star) identify canonical NF9-specific TCRs, with other clonotypes included for comparison. **B.** Heatmap summarising Jurkat reporter cell activation for each TCR in (A) against single amino acid substitutions at position 5 of the NF9 peptide. Responses are normalised to each TCR's maximal activation to enable parallel comparison. **C.** Titration assays of each TCR from (A) expressed in Jurkat cells, tested against the position 5 variants recognised in (B), as well as the 5R (L452R) escape mutant and the 6F (Y453F) variant identified in farmed mink (37).

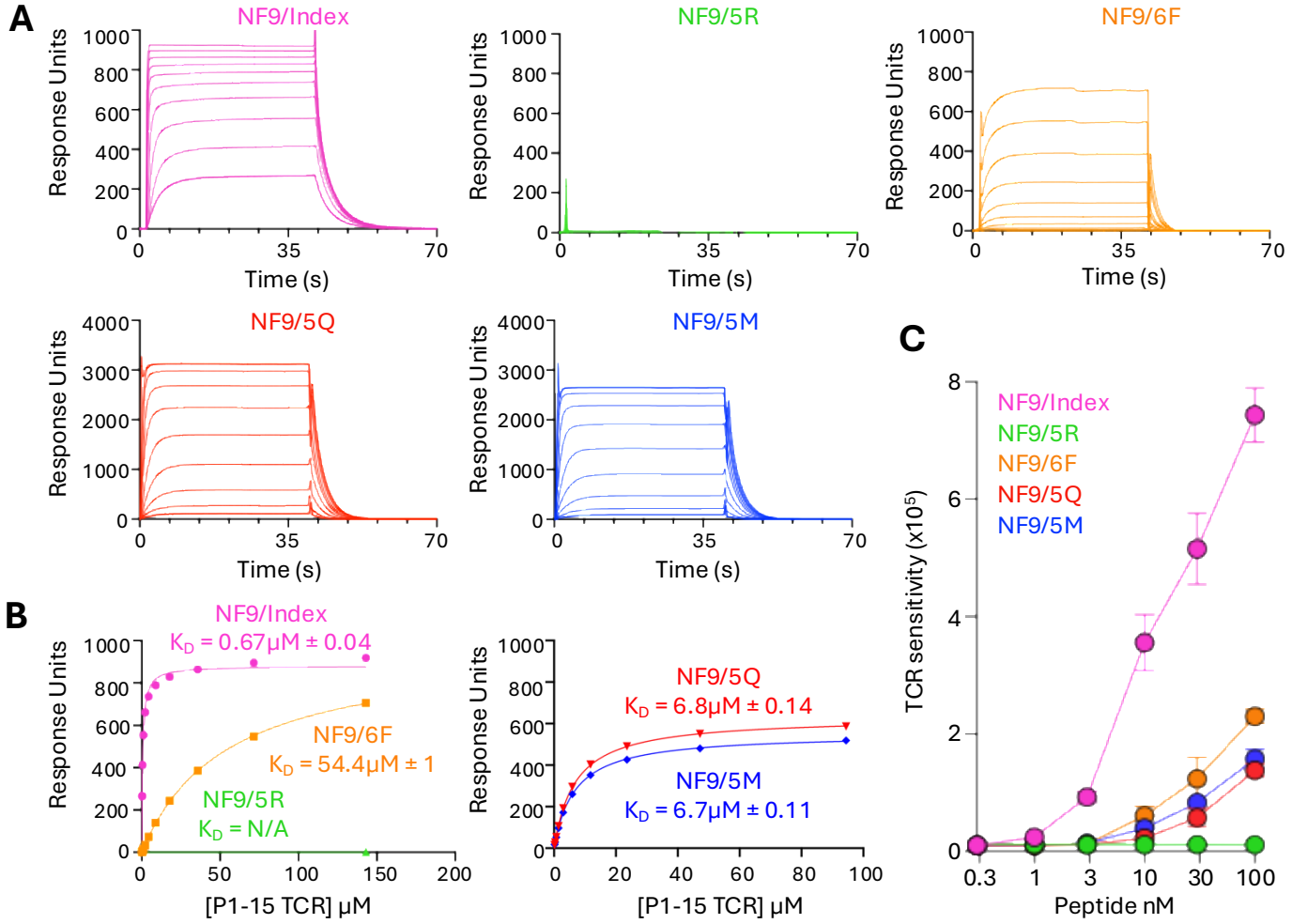

Figure 4. Binding affinity and cross-reactivity of P1-15:A24/NF9 interaction.
A. Surface Plasmon resonance (SPR) analysis of P1-15 TCR binding to HLA-A*24:02 complexes presenting NF9 (magenta), NF9-6F (orange), NF9-5R (green), NF9-5Q (red) and NF9-5M (blue). **B**. SPR responses to ten serial dilutions of P1-15 TCR were measured. K_Ds were determined by non-linear fit curve (y= [P1 x]/[P2 + x]). **C.** NFAT-luciferase reporter activity in Jurkat cells transduced with P1-15 TCR and stimulated with NF9 or variant peptides (NF9-5R, NF9-6F, NF9-5Q, and NF9-5M), demonstrating functional sensitivity corresponding to the measured binding affinities.

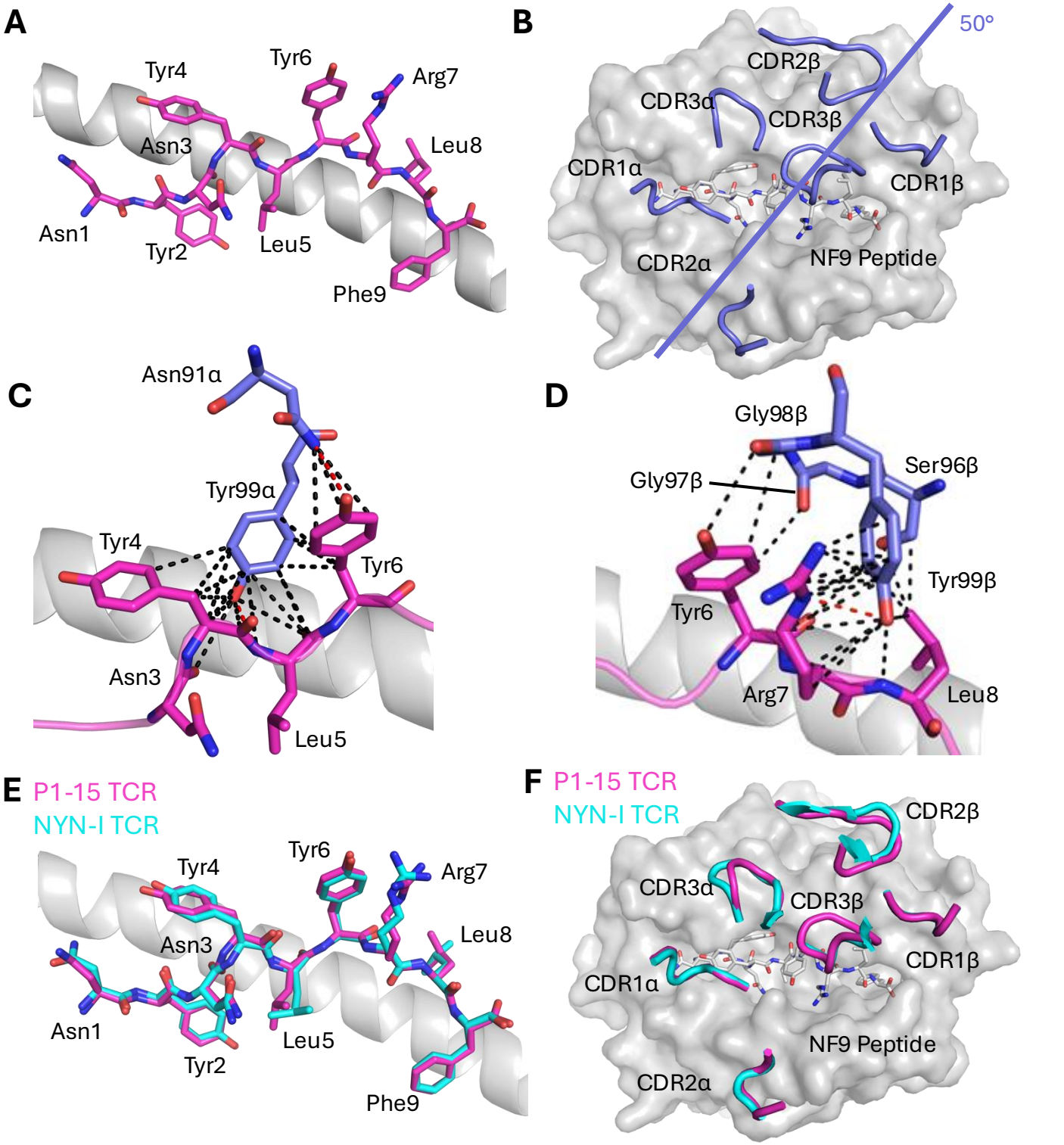

Figure 5. Structural analysis of the public P1-15 TCR/NF9-A24 complex
A. Presentation of the NF9 peptide (magenta sticks) when in complex with the P1-15 TCR. **B.** Top-down view of the NF9 peptide (white sticks) showing the distribution of the P1-15 CDR loops (blue cartoon). The crossing angle is indicated by the blue line. **C-D** Detailed vies of contacts between CDR1α (C), CDR3β (D) and CDR3α and the NF9 peptide (magenta sticks) showing Van der Waals (black dotted lines) and hydrogen (red dotted lines) interactions. **E**. Structural comparison of the NF9 peptide (sticks) bound to P1-15 TCR (magenta) or NYN-I TCR (cyan). **F.** Top-down comparison of the P1-15 (blue cartoon) and NYN-I (cyan cartoon) CDR loop distributions over the NF9 peptide (white sticks).

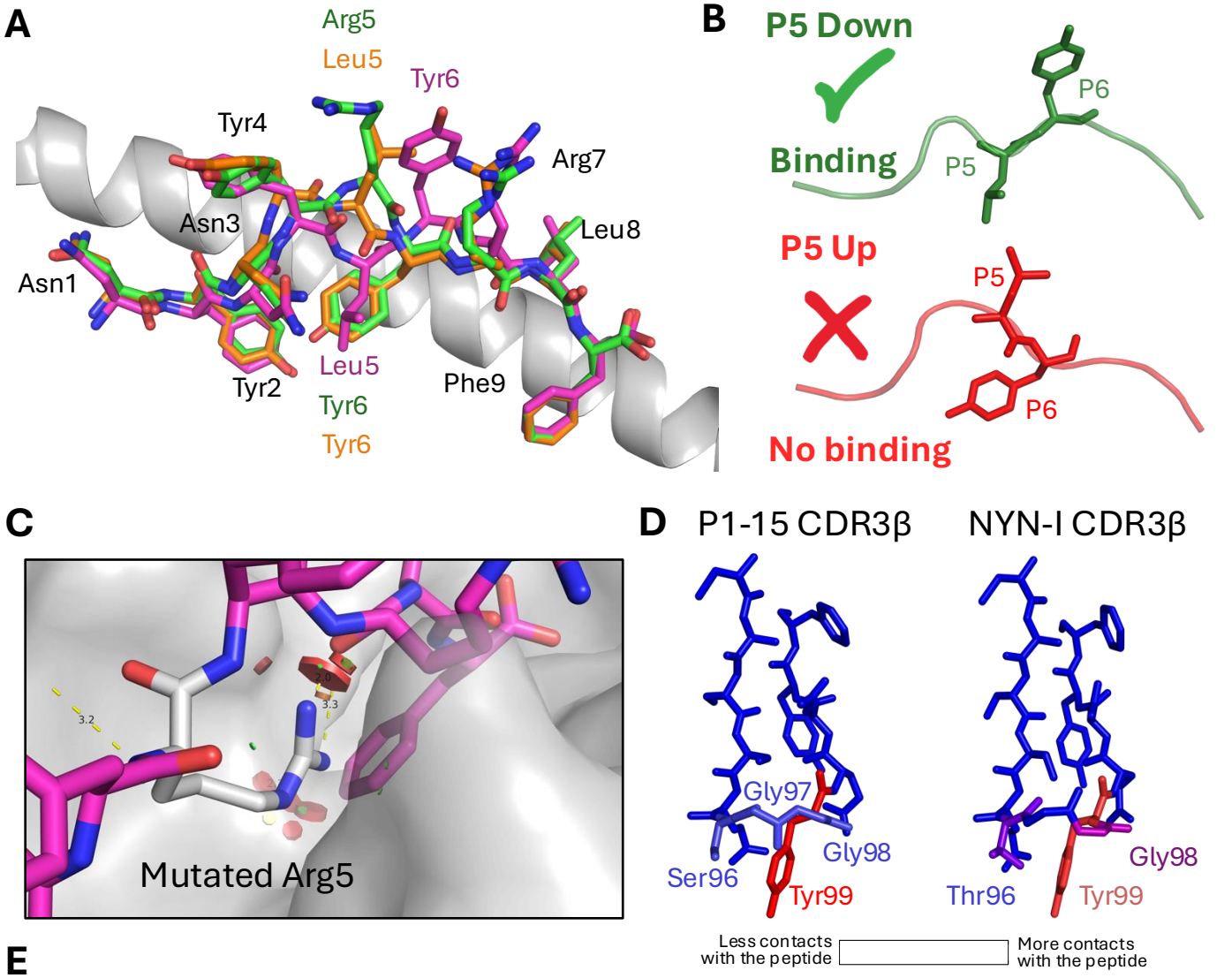

Figure 6. Structural basis for position-5-driven reorientation of the NF9 peptide within HLA-A*24:02. **A**. A24/NF9 peptide (magenta sticks) in complex with the P1-15 TCR, with uncomplexed A24/NF9-6F (orange sticks) and A24/NF9-5R (green sticks) structures superimposed, demonstrating side-chain flipping at positions 5 and 6. **B**. Diagram illustrating the alternative "P5-up" (top, green) and "P5-down" (bottom, red) peptide orientations adopted within the peptide–HLA complexes in **A**. **C**. Modelling of the NF9 peptide residue 5 (white sticks) mutated to arginine using PyMOL. Red discs indicate steric clashes; the displayed rotamer produced the fewest clashes after PyMOL energy minimisation. **D.** Structural heatmap showing the number and distribution of atomic contacts between each of the P1-15 and NYN-I TCRs and the NF9 peptide. These bonds are also shown in **E,** a schematic representation of intermolecular contacts between NF9 peptide residues and the P1-15 (top) or NYN-I (bottom) TCRs, showing how CDR3 tyrosines dominate the molecular contacts with both HLA and peptide. In **D** blue = no peptide and red = highest contacts with the colors reflecting P1-15 binds much stronger than NYN-1 (K_D ≈ 0.67 μM vs > 10 μM).

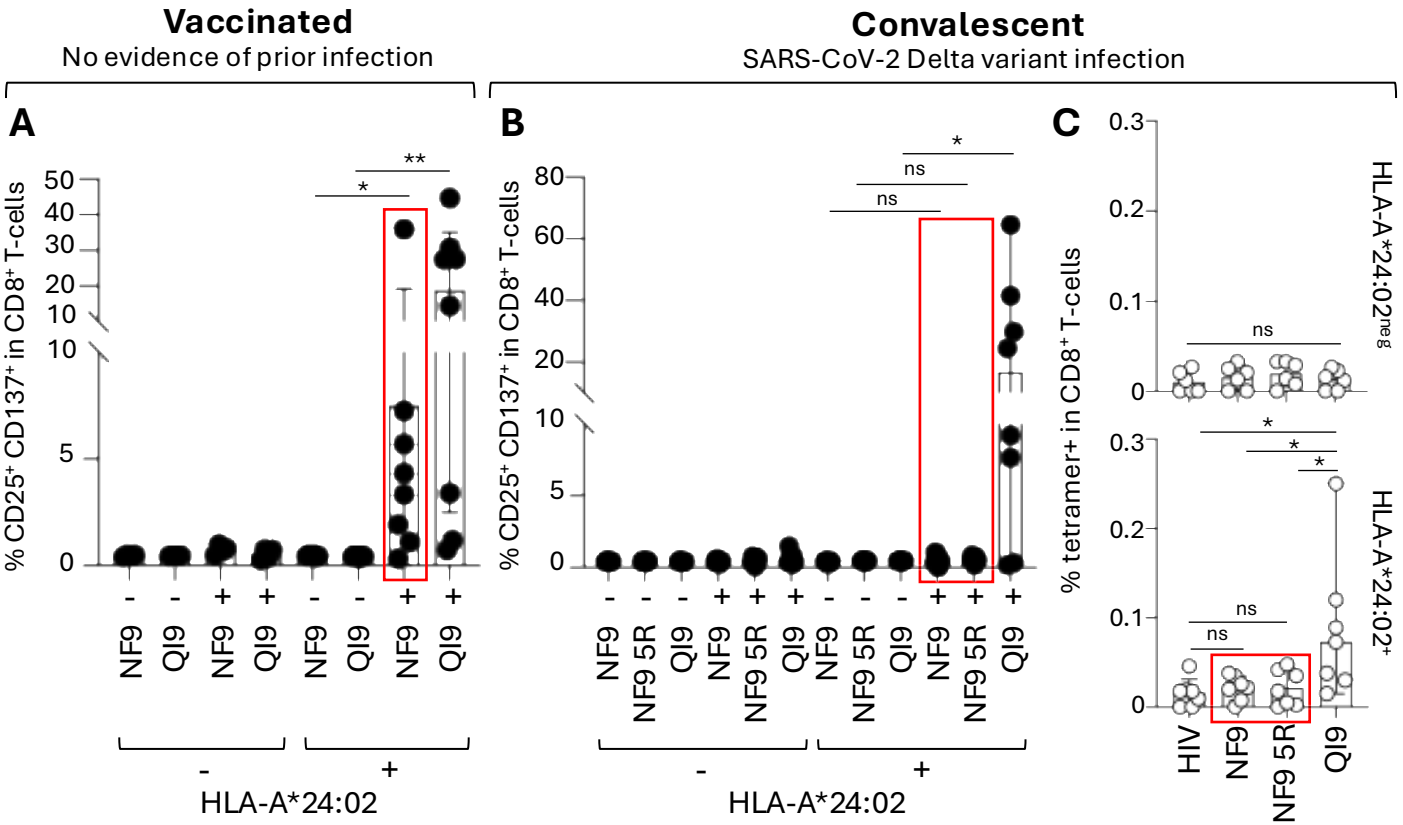

Figure 7. NF9-5R-specific T-cells are not detectable in SARS-CoV-2 Delta-infected convalescents. A. Activation-induced marker assay of PBMCs from vaccinated donors with no evidence of prior SARS-CoV-2 infection. Cells were stimulated for 14 days with A24/NF9 (NYNYLYRLF448–456) or A24/QI9 (QYIKWPWYI1208–1216) peptides. Data show the percentage of $CD25^+CD137^+$ $CD8^+$ T-cells in HLA-A*24:02-negative (n = 4) and HLA-A*24:02$^+$ (n = 8) donors. Wilcoxon matched-pairs signed-rank test (*p = 0.0156, **p = 0.0078). **B**. Activation-induced marker assay of PBMCs from unvaccinated convalescents infected with the SARS-CoV-2 Delta variant. Cells were stimulated with A24/NF9, A24/NF9-5R, or A24/QI9 peptides. Data show the percentage of $CD25^+CD137^+$ $CD8^+$ T-cells in HLA-A*24:02-negative (n = 9) and A*24:02$^+$ (n = 8) donors. Wilcoxon matched-pairs signed-rank test (*p = 0.0391). C. *Ex vivo* detection of HLA-A*24:02-restricted tetramer$^+$ $CD8^+$ T-cells in Delta-infected convalescents. PBMCs from HLA-A*24:02-negative (n = 6) and A*24:02$^+$ (n = 7) donors were stained with tetramers specific for HIV-KW9 (negative control), A24/NF9, A24/NF9-5R, or A24/QI9. Wilcoxon matched-pairs signed-rank test (*p = 0.0156 vs A24/HIV-KW9 and A24/NF9-5R and *p = 0.0312 vs A24/NF9).

SUPPLEMENTAL DATA

Position-5-Driven Reorientation of an Immunodominant HLA-A*24:02 SARS-CoV-2 Epitope Drives Universal T-cell Escape

Takashi Nakama[1†], Aaron Wall[2†], Garry Dolton[2#], Li-Rong Tan[2], Hannah Thomas[2], Hiroshi Hamana[3], Yoshiki Aritsu[1], Toong Seng Tan[1], Mako Toyoda[1], Yoshihiko Goto[1], Huanyu Li[1], Mizuki Kitamatsu[4], Keiko Udaka[5], Yusuke Miyashita[6, 7], Hiroyuki Oshiumi[6], Kimitoshi Nakamura[7], Yoji Nagasaki[8], Rumi Minami[9], Hirotomo Nakata[10], Pierre J Rizkallah[2], Hiroyuki Kishi[3], Takamasa Ueno[1], Andrew K. Sewell[1,2‡*], Chihiro Motozono[1‡*]

[1] Division of Infection and Immunity, Joint Research Center for Human Retrovirus infection, Kumamoto University, Kumamoto 8600811, Japan
[2] Division of Infection and Immunity, Cardiff University School of Medicine, CF14 4XN Cardiff, Wales, UK
[3] Department of Immunology, Faculty of Medicine, Academic Assembly, University of Toyama, Toyama 9300194, Japan
[4] Department of Applied Chemistry, Faculty of Science and Engineering, Kindai University, Osaka 577-8502, Japan
[5] Department of Immunology, Kochi University, Kochi 7838505, Japan
[6] Department of Immunology, Graduate School of Medical Sciences, Faculty of Life Sciences, Kumamoto University, Kumamoto 8608556, Japan
[7] Department of Pediatrics, Graduate School of Medical Sciences, Kumamoto University, Kumamoto 8608556, Japan
[8] Division of Infectious Diseases, Clinical Research Institute, National Hospitalization Organization, Kyushu Medical Center, Fukuoka 8108563, Japan
[9] Internal Medicine, Clinical Research Institute, National Hospital Organization, Kyushu Medical Center, Fukuoka 8108563, Japan
[10] Department of Hematology, Rheumatology and Infectious Diseases, Kumamoto University School of Medicine, Kumamoto University Hospital, Kumamoto 8608556, Japan

Prepared by Andrew Sewell
March 6th, 2026

CONTENTS

Table S1: Donor information related to Fig. 1, 2 and 7.

Donor ID	Sex	Age	HLA-A24?	vaccinated?	Days after 2nd vax	Blood collection
VKU-1	Male	48	Positive	BNT162b2	35	03/05/2021
VKU-2	Male	37	Positive	BNT162b2	35	03/05/2021
VKU-3	Male	40	Positive	BNT162b2	35	03/05/2021
VKU-5	Male	34	Negative	BNT162b2	35	03/05/2021
VKU-7	Male	55	Positive	BNT162b2	31	08/05/2021
VKU-8	Male	55	Negative	BNT162b2	35	08/05/2021
VKU-10	Female	60	Positive	BNT162b2	48	03/05/2021
VKU-11	Female	39	Positive	BNT162b2	34	25/05/2021
VKU-16	Male	54	Negative	BNT162b2	35	08/05/2021
VKU-17	Male	35	Negative	BNT162b2	35	25/05/2021
VKU-18	Female	38	Positive	BNT162b2	35	25/05/2021
VKU-19	Female	36	Positive	BNT162b2	35	27/05/2021
VKU-20	Male	33	Negative	BNT162b2	34	25/05/2021
VKU-21	Female	27	Negative	BNT162b2	34	25/05/2021
VKU-22	Male	34	Positive	BNT162b2	36	27/05/2021
VKU-23	Male	54	Positive	BNT162b2	49	27/05/2021
VKU-25	Male	46	Negative	BNT162b2	34	25/05/2021
VKU-27	Male	43	Negative	BNT162b2	35	27/05/2021
VKU-28	Male	30	Positive	BNT162b2	35	10/06/2021
VKU-41	Male	34	Negative	BNT162b2	35	27/05/2021
VKU-42	Male	34	Positive	BNT162b2	35	27/05/2021
VKU-43	Male	38	Negative	BNT162b2	35	27/05/2021
VKU-44	Male	29	Positive	BNT162b2	31	25/05/2021
VKU-45	Male	27	Negative	BNT162b2	35	27/05/2021
VKU-46	Female	40	Negative	BNT162b2	35	27/05/2021
VKU-47	Female	57	Negative	BNT162b2	31	25/05/2021
VKU-48	Male	59	Positive	BNT162b2	35	27/05/2021
GV9	Female	24	Positive	BNT162b2	202	27/12/2021
GV12	Female	28	Negative	BNT162b2	23	01/07/2021
GV15	Female	23	Positive	BNT162b2	182	06/01/2022
GV16	Male	22	Positive	No	NA	17/05/2021
GV16-1	Male	22	Positive	BNT162b2	202	27/12/2021
GV17	Male	24	Negative	BNT162b2	21	29/06/2021
GV19	Male	24	Positive	BNT162b2	202	27/12/2021
GV24	Male	23	Positive	BNT162b2	212	06/01/2022
GV25	Male	24	Negative	BNT162b2	22	30/06/2021
GV26	Male	23	Positive	BNT162b2	212	06/01/2022
GV27	Female	23	Negative	BNT162b2	21	29/06/2021
GV32	Male	56	Positive	No	NA	11/05/2021
GV32-1	Male	56	Positive	BNT162b2	27	05/07/2021
GV32-2	Male	56	Positive	BNT162b2	195	20/12/2021
GV33	Male	39	Positive	No	NA	11/05/2021
GV33-1	Male	39	Positive	BNT162b2	24	28/07/2021
GV33-2	Male	39	Positive	BNT162b2	192	20/12/2021
GV34	Female	38	Positive	BNT162b2	24	05/07/2021
GV35	Male	52	Positive	BNT162b2	24	05/07/2021
GV36	Male	41	Positive	BNT162b2	21	05/07/2021
GV36-1	Male	41	Positive	BNT162b2	192	20/12/2021
GV52	Female	67	Positive	BNT162b2	21	05/07/2021
GV59	Male	37	Positive	BNT162b2	25	15/09/2021
GV59-1	Male	37	Positive	BNT162b2	126	20/12/2021
GV60	Male	51	Positive	mRNA-1273	116	20/12/2021

Table S2: Convalescent donor information related to Fig. 2 and 6.

Cohort	Donor ID	Sex	Age	HLA-A24?	vaccinated?	COVID-19 severity	Days post PCR+ or onset	Blood collection
A24+ COVID-19 convalescents	KK-008	Male	63	Positive	No	Mild	17	19/08/2021
	GV-38	Male	23	Positive	No	Mild	18	20/05/2021
	GV-41	Male	33	Positive	No	Mild	16	20/05/2021
	GV-42	Male	25	Positive	No	Mild	32	03/06/2021
	AK-16	Female	46	Positive	No	Moderate	11	27/08/2021
	AK-18	Female	25	Positive	No	Moderate	10	03/09/2021
	AK-20	Female	58	Positive	No	Severe	NA	03/09/2021
	AK-24	Female	28	Positive	No	Severe	13	08/09/2021
	AK-25	Female	42	Positive	No	Severe	7	08/09/2021
	IK-25	Male	61	Positive	NA	Moderate	7	09/03/2022
	IK-26	Female	40	Positive	NA	Moderate	17	06/08/2021
	IK-32	Male	36	Positive	NA	Moderate	19	01/09/2021
A24- COVID-19 convalescents	AK-12	Male	53	Negative	No	Moderate	11	25/08/2021
	AK-19	Male	47	Negative	No	Severe	11	03/09/2021
	AK-32	Male	57	Negative	No	Moderate	10	13/09/2021
	IK-21	Female	71	Negative	NA	Moderate	16	30/07/2021
	IK-22	Male	33	Negative	NA	Mild	14	30/07/2021
	IK-24	Male	43	Negative	NA	Moderate	17	06/08/2021
	IK-27	Female	56	Negative	NA	Moderate	13	06/08/2021
	IK-33	Male	41	Negative	NA	Mild	34	06/09/2021
	IK-34	Male	38	Negative	NA	Mild	46	16/09/2021

NA – Not applicable

Table S3: HLA binding of NF9-5X peptides.

Name	Sequence	Normalized log Kd
NF9 (WT)	NYNY**L**YRLF	-6.83
NF9-5A	----**A**----	-6.90
NF9-5C	----**C**----	-6.12
NF9-5D	----**D**----	-6.17
NF9-5E	----**E**----	-5.90
NF9-5F	----**F**----	-6.72
NF9-5G	----**G**----	-6.56
NF9-5H	----**H**----	-6.93
NF9-5I	----**I**----	-7.03
NF9-5K	----**K**----	-6.94
NF9-5M	----**M**----	-6.85
NF9-5N	----**N**----	-7.00
NF9-5P	----**P**----	-6.82
NF9-5Q	----**Q**----	-6.55
NF9-5R	----**R**----	-6.35
NF9-5V	----**V**----	-6.68
NF9-5S	----**S**----	-6.62
NF9-5T	----**T**----	-6.71
NF9-5V	----**V**----	-6.68
NF9-5W	----**W**----	-6.14
NF9-5Y	----**Y**----	-6.50

Colors of text in name column match those used elsewhere in this study

Table S4: Crystallography statistics for X-ray crystallography structures in this study

PDB Entry	**28IL**	**8RJH**	**8RJI**
Protein	**P1-15:HLA A*2402-NF9**	**HLA A*2402-NF9_6F**	**HLA A*2402-NF9_5R**
Data Collection			
Diamond Beamline	I04	I04	I04
Date	28-04-2022	28-04-2022	28-04-2022
Wavelength	0.9795	0.9795	0.9795
Crystal Data (outer shell statistics in brackets)			
Crystallisation Conditions	0.1 M di-Sodium malonate, 0.1 M HEPES, 30% w/v Poly(acrylic acid sodium salt) 2,100, pH7	0.1M Sodium cacodylate, 20% PEG 4000, 15% Glycerol, pH 6	0.1M MES, 20% PEG 4000, 15% Glycerol, pH 7
a,b,c (Å)	200.44, 200.44, 156.27	344.8, 84.34, 91.45	103.28, 77.02, 111.82
α,β,γ (°)	90.0, 90.0, 120.0	90.00, 102.14, 90.00	90.00, 110.58, 90.00
Space group	P 3_1 2 1	C 1 2 1	P 1 2_1 1
Resolution (Å)	3.1 – 60.49	2.60 – 86.92	2.3 – 54.8
Outer shell	3.10 – 3.18	2.60 – 2.65	2.3 – 2.35
R-merge (%)	0.287 (3.769)	0.166 (1.581)	0.144 (1.088)
R-pim	0.091 (1.171)	0.101 (1.021)	0.089 (0.686)
R-meas (%)	0.300 (3.941)	0.195 (1.887)	0.170 (1.289)
CC1/2	0.997 (0.407)	0.995 (0.465)	0.996 (0.677)
I / σ(I)	8.8 (0.9)	7.7 (1.0)	8.0 (1.5)
Completeness (%)	100 (100)	100 (99.5)	99.6 (96.3)
Multiplicity	21 (22)	7.1 (6.6)	7.0 (6.9)
Total Measurements	1,387,790 (101,844)	564,978 (29,665)	512,213 (29,794)
Unique Reflections	65,958 (4,631)	79,258 (4,490)	73,135 (4,344)
Wilson B-factor(Å^2)	93	51.1	33.7
Refinement Statistics			
Non-H Atoms	14,898	19,159	13,033
R-work reflections	62481	75,257	73,254
R-free reflections	3,218	3,967	3,602
R-work/R-free (%)	19.0 / 23.1	22.4 / 26.4	21.7 / 26.5
rms deviations (ML target in brackets)			
Bond lengths (Å)	0.006 (0.012)	0.010 (0.013)	0.012 (0.013)
Bond Angles (°)	1.504 (1.772)	1.372 (1.648)	1.447 (1.647)
[1]Coordinate error	0.355	0.323	0.4401
Mean B value (Å^2)	112.3	63.2	39.2
Ramachandran Statistics			
Favoured/Outliers	1459 / 20	2152 / 1	1429 / 6
%	89 / 1	95 / 0	94 / 0

* One crystal was used for determining each structure.

[1] Coordinate Estimated Standard Uncertainty in (Å), calculated based on maximum likelihood statistics.

Table S5. Molecular contacts between the P1-15 T-cell Receptor and the A24/NF9 peptide:MHC complex. Note that the P1-15 TCR β-chain construct contained a short N-terminal extension resulting from the expression system, and the PDB numbering therefore begins from the first residue of this construct. For consistency with the published literature (e.g., PDB: 8YE4), amino acid numbering in this manuscript follows the canonical TCR sequence i.e., -3 relative to the PDB files for the β chain.

CDR loop	TCR residue	Peptide residue	MHC residue	VdWs (≤4 Å)	H-bonds (≤3.4 Å)
CDR1α	Ala29	Tyr4		3	
	Gln31		Gln155	2	
		Tyr4		8	
		Tyr6		1	
	Ser32	Tyr6		2	
CDR2α	Tyr51		Ala150	1	
			His151	23	
			Glu154	1	
	Ser52		Glu154	2	
	Ser53		Glu154	4	
FWα	Arg66		Ala158	3	
CDR3α	Asn91	Tyr6		4	
	Leu93		Glu62	1	
			Gly65	2	
			Lys66	3	
	Asn95		Gly65	1	
	Ser96		Gly65	1	
			Gly68	1	
	Tyr98		Lys66	2	
			Ala69	1	
		Asn3		1	
		Tyr4		8	
		Leu5		5	1
		Tyr6		4	
CDR1β	Asn30		Glu76		1
CDR3β	Ser96	Leu8		2	
	Gly97	Tyr6		1	
	Gly98	Tyr6		2	
	Tyr99	Tyr6		1	
		Arg7		12	1
		Leu8		5	

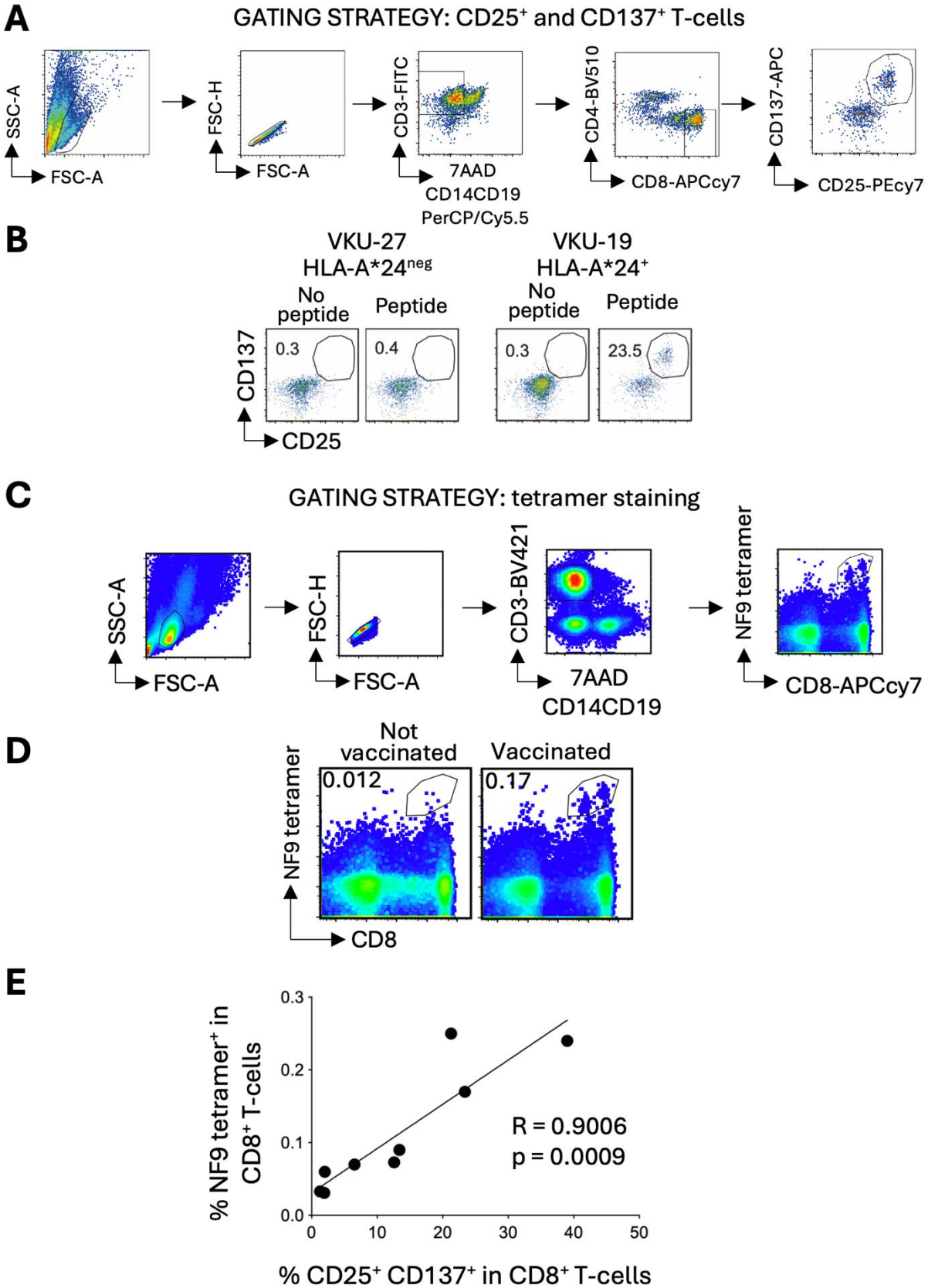

Supplemental Figure S1. Flow cytometry gating strategies, representative flow cytometry plots, and correlation between activation status and tetramer staining for the HLA-A*24:02 NF9 epitope. (**A**) Flow cytometry gating strategy of $CD25^+CD137^+$ T-cell lines from donor VKU19. (**B**) $CD8^+CD25^+CD137^+$ data for an HLA-A*24:02 positive and negative donor. (**C**) HLA-A*24:02 NF9 tetramer staining of PBMCs from donor VKU-19. (**E**) Correlation between the frequency of $CD25^+CD137^+CD8^+$ activated T cells and that of HLA-A*24:02 NF9 $tetramer^+CD8^+$ T cells in HLA-$A*24:02^+$ vaccinated donors (n = 9). R = 0.9006 and *** p = 0.0009 by two-tailed Person test.

GV33

TRAV	TRAJ	CDR3α	TRBV	TRBD	TRBJ	CDR3β	%
12-1*01	41*01	CVVNLLNSNSGYALNF	6-1*01	2*01	2-7*01	CASSEAGGYEQYF	12.5
14/DV4*02	45*01	CAMREPPLIRGADGLTF	2*01	1*01	2-7*01	CASSEGQGYEQYF	8.3
14/DV4*02	50*01	CAMRELGVKTSYDKVIF	6-1*01	2*02	2-7*01	CASSEGRGYEQYF	4.2
8-6*02	17*01	SPGAAGNKLTF	6-1*01	2*01	2-7*01	CASSETGGYEQYF	4.2
16*01	6*01	CALSGPSGAGGSYIPTF	5-4*01	2*01	2-7*01	CASSETSGYEQYF	4.2
12-2*01	20*01	CAVTHLARADYKLSF	5-1*01	1*01	2-7*01	CASSDRTGYEQYF	4.2
12-1*01	5*01	CVVKGTGRRALTF	11-1*01	1*01	2-7*01	CASSLWQGYEQFF	4.2
21*02	47*01	CAVNSYGNKLVF	5-1*01	1*01	2-7*01	CASSPGTGYEQYF	4.2
4*01	36*01	CLVGDGGGANNLFF	4-1*01	2*01	2-7*01	CASSQSLGYEQYF	4.2
12-2*02	35*01	CAVNGFGNVLHC	10-1*01	2*01	2-7*01	CASSESIAYEQYF	4.2
21*02	26*01	CAVPNNYGQNFVF	2*01	1*01	2-7*01	CASSEFGVGYEQYF	4.2
12-2*01	40*01	CAVNSGTYKYIF	5-1*01	1*01	2-7*01	CASSEGAGGYEQYF	4.2
12-1*01	8*01	CVVSTPLMNTGFQKLVF	6-1*01	1*01	2-7*01	CASSEGQGPYEQYF	4.2
26-2*01	32*02	CILFYGGATNKLIF	2*01	1*01	2-7*01	CASSEGQLPYEQYF	4.2
14/DV4*02	52*01	CAIVGGTSYGKLTF	19*01	1*01	2-7*01	CASSLAEGTEQYF	4.2
27*01	23*01	CAGARNQGGKLIF	27*01	1*01	1-1*01	CASSLGGHNPEEAFF	4.2
23/DV6*01	45*01	CAAGSGGGADGLTF	2*01	2*02	2-7*01	CASNFEGGSSYEQYF	4.2
17*01	20*01	CATAPWDYKLSF	5-6*01	1*01	1-1*01	CASSLGQGTEAFF	4.2
17*01	40*01	CATVTYKYIF	5-4*01	-	2-7*01	CASSLGSADEQYF	4.2
1-1*01	4*01	CAAASGGYNKLIF	27*01	1*01	2-1*01	CASSLSLGEQFF	4.2
12-1*01	9*01	CVVTLYTGGFKTIF	7-9*03	1*01	1-1*01	CASSPQGADEAFF	4.2

GV34

TRAV	TRAJ	CDR3α	TRBV	TRBD	TRBJ	CDR3β	%
13-1*02	44*01	SRNTGTASKLTF	5-1*01	1*01	2-7*01	CASSFGQGYEQYF	8.6
12-1*01	33*01	CVVNALMDSNYQLIW	5-1*01	1*01	2-7*01	CASSLGQGYEQYF	5.7
12-1*01	33*01	CVVNLFDSNYQLIW	2*01	1*01	2-7*01	CASSEGAGYEQYF	2.9
12-1*01	28*01	CVVNMLYSGAGSYQLTF	6-1*01	2*01	1-1*01	CASSESAGYEAFF	2.9
12-1*01	28*01	CVVNVPLGGAGSYQLTF	6-4*01	1*01	2-7*01	CASSEGQGYEQYF	2.9
12-1*01	41*01	CVVNGRRNSGYALNF	10-1*01	-	2-7*01	CASSESFGYEQYF	2.9
12-1*01	28*01	CVVNKLDSGAGSYQLTF	5-1*01	2*01	2-7*01	CASSLAGGYEQYF	2.9
12-1*01	8*01	CVVNDRWNTGFQKLVF	2*01	1*01	2-7*01	CASSEGQAYEQYF	2.9
12-1*01	8*01	CVAREGFQKLVF	9*01	2*01	2-7*01	CASSETPAYEQYF	2.9
5*01	32*01	CAPRGATTKLIF	6-1*01	1*01	2-7*01	CASSEFQGYEQYF	2.9
29/DV5*04	54*01	CAASVIQGAQKLVF	4-1*01	1*01	2-7*01	CASSPGRSYEQYF	2.9
20*04	49*01	CAVPGYSRATGNQLTF	2*01	1*01	2-7*01	CASMVGLTYEQYF	2.9
38-2/DV8*01	42*01	CAYRSAWWGPSQGNLIF	3-1*01	1*01	2-7*01	CASSWGQDAYEQYF	2.9
5*01	42*01	CAESGGSQGNLIF	5-1*01	1*01	2-7*01	CASMGQNYEQYF	2.9
21*01	58*01	CAVRPETSGSRLTF	6-5*01	2*01	2-1*01	CASSALGLAAYNEQFF	2.9
27*01	35*01	CAGAVGFGNVLHC	2*01	1*01	1-2*01	CASSEAGAVYGYTF	2.9
17*01	52*01	CATTNAGGTSYGKLTF	2*01	2*02	2-7*01	CASSEWVGSSYEQYF	2.9
8-6*02	18*01	CAVSDRGSTLGRLYF	28*01	1*01	1-1*01	CASSFGAYDTEAFF	2.9
12-2*01	54*01	CAVNTGAQKLVF	6-6*01	1*01	2-1*01	CASSFPTAGGARNEQFF	2.9
17*01	8*01	CATDRMNTGFQKLVF	19*01	1*01	2-7*01	CASSIGQTPTYEQYF	2.9
20*02	39*01	CAVQNNNAGNMLTF	5-1*01	1*01	1-1*01	CASSLESGTEAFF	2.9
12-3*01	57*01	CAMSIQGGSEKLVF	5-6*01	2*02	1-5*01	CASSLGSSAQHF	2.9
8-6*01	11*01	CAVRRYSTLTF	5-6*01	1*01	2-7*01	CASSLQGARPYEQYF	2.9
17*01	17*01	CALGGAAGNKLTF	13*01	-	2-3*01	CASSLTDTQYF	2.9
29/DV5*04	39*01	CAANDAGNMLTF	4-1*01	2*01	2-7*01	CASSQDPALAGPYEQYF	2.9
10*02	15*01	CVVSARLNTDAASNLTF	11-3*01	1*01	2-1*01	CASSSRARPNEQFF	2.9
30*05	34*01	CGTALPYNTDKLIF	7-2*02	2*01	2-5*01	CASSSRTDLKETQYF	2.9
5*01	44*01	CAETKKNTGTASKLTF	7-6*01	1*01	2-5*01	CASSSSRSGITQYF	2.9
19*01	36*01	CALSESGANNLFF	7-9*01	1*01	2-5*01	CASSSWRQQETQYF	2.9
5*01	30*01	CVVMNRDDKIIF	6-2*01	2*01	2-1*01	CASSYSAGEQFF	2.9
12-1*01	12*01	CVVITMDSSYKLIF	20-1*01	1*01	2-7*01	CSARPRQGVYEQYF	2.9
12-2*01	54*01	CAVNEIQGAQKLVF	29-1*01	1*01	2-5*01	CSVTPGGETQYF	2.9

VK22

TRAV	TRAJ	CDR3α	TRBV	TRBD	TRBJ	CDR3β	%
4*01	3*01	CLVGGSYSSASKIIF	2*01	1*01	2-7*01	CASSEGRGYEQYF	13.0
12-1*01	33*01	CVVNVYMDSNYQLIW	2*01	2*01	2-7*01	CASSESAGYEQYF	4.3
12-1*01	28*01	CVVNMLGSGAGSYQLTF	5-4*01	2*02	2-7*01	CASSLAGGYEQYF	4.3
12-1*01	33*01	CVVNGDSNYQLIW	4-1*01	1*01	2-7*01	CASSQQHGYEQYF	4.3
12-1*01	42*01	CVVTGGSQGNLIF	20-1*02	2*01	2-7*01	CSARDWLGTSDYEQYF	4.3
6*03	47*01	CALAEYGNKLVF	6-5*01	-	2-7*01	CASSYSFSYEQYF	4.3
29/DV5*04	37*01	CAAPGTSGNTGKLIF	15*02	1*01	2-7*01	CATSRILGYEQYF	4.3
5*01	20*01	CAETPSRGLSF	4-1*01	2*01	2-7*01	CASSQDEAGEQYF	4.3
2*01	11*01	CAVEGYSGYSTLTF	12-4*01	2*01	1-1*01	CASLSGEAFF	4.3
20*02	42*01	CALQTNYGGSQGNLIF	9*01	2*02	2-1*01	CASSAGLEGGGTYNEQFF	4.3
24*01	32*02	CASYGGATNKLIF	2*01	2*01	2-7*01	CASSEFRGATYEQYF	4.3
38-2/DV8*01	43*01	CALNQNNNDMRF	12-3*01	2*02	2-3*01	CASSLTAGGPRTRTQYF	4.3
12-2*02	9*01	CAVRGFKTIF	12-3*01	1*01	2-1*01	CASSPAPGSGGNEQFF	4.3
12-2*02	20*01	CAVTNDYKLSF	6-5*01	2*01	2-3*01	CASSPHLGGGEDTQYF	4.3
26-1*01	23*01	CIVDPWGGGKLIF	9*01	1*01	1-1*01	CASSSSRQGNTEAFF	4.3
20*02	18*01	CAVQVWDRGSTLGRLYF	30*01	1*01	1-1*01	CAWSIQPGGTEAFF	4.3
3*01	6*01	CAVRDIRGSYIPTF	30*01	1*01	1-1*01	CAWSVQNTEAFF	4.3
13-1*02	20*01	CAASLAGNDYKLSF	20-1*05	2*01	2-7*01	CSARDRVRIYEQYF	4.3
4*01	5*01	CLVYRRALTF	29-1*01	1*01	1-1*01	CSVGDGNTEAFF	4.3
12-2*02	49*01	CAVNTPITNTGNQFYF	29-1*01	-	2-7*01	CSVTRSYEQYF	4.3
41*01	58*01	CAVPTSGYRLTF	9*03	2*02	2-5*01	CTSSKPAGGNTQYF	4.3

VK48

TRAV	TRAJ	CDR3α	TRBV	TRBD	TRBJ	CDR3β	%
12-1*01	28*01	CVVNRLQSGAGSYQLTF	2*01	2*01	2-7*01	CASSEAGGYEQYF	11.1
4*01	9*01	CLVGDIRHTGGFKTIF	2*01	-	1-6*02	CASSEDSPLHF	11.1
12-1*01	53*01	CVVNTLNSGGSNYKLTF	4-2*01	1*01	2-7*01	CASSPTGGYEQYF	5.6
12-1*01	12*01	CVVTVPPAMDSSYKLIF	6-1*01	1*01	2-7*01	CASSRKDGYEQYF	5.6
12-1*01	41*01	CVVNMLAGNSGYALNF	2*01	1*01	2-7*01	CASSDQQGYEQYF	5.6
12-1*01	33*01	CVVNILRDSNYQLIW	25-1*01	1*01	2-7*01	CASSEGQGYEQYF	5.6
12-1*01	20*01	CVVNCLREDDYKLSF	6-1*01	2*02	2-7*01	CASSEGRGYEQYF	5.6
16*01	4*01	CALSLFSGGYNKLIF	4-1*01	1*01	2-7*01	CASSQGQGYEQYF	5.6
23/DV6*02	49*01	CPAGGNQFYF	6-1*01	1*01	2-7*01	CASSEWVGYEQYF	5.6
17*01	20*01	CATDTNDYKLSF	19*01	1*01	1-2*01	CASSMRGQGYGYTF	5.6
20*02	4*01	CAVQPSFSGGYNKLIF	2*01	1*01	2-7*01	CASSEGQGPYEQYF	5.6
27*01	37*01	RAGAGGGTGELTF	6-1*01	1*01	1-5*01	CASSEWGIGDNQPQHF	5.6
27*01	42*01	CAASMGGSQGNLIF	11-2*01	1*01	2-4*01	CASSLGPVLAKNIQYF	5.6
14/DV4*02	29*01	CAMRPNSGNTPLVF	4-1*01	1*01	2-7*01	CASSQGRQGAAYEQYF	5.6
8-6*02	37*02	CAVSDRASNTGKLIF	4-1*01	1*01	1-1*01	CASSQVTGGWTEAFF	5.6
23/DV6*01	28*01	CAASTPGAGSYQLTF	6-5*01	1*01	2-7*01	CASSSSVQDIVEF	5.6
12-3*01	54*01	CAMRAPGAQKLVF	9*02	2*01	2-7*01	CASSVGPGLAAYEQYF	5.6

GV36

TRAV	TRAJ	CDR3α	TRBV	TRBD	TRBJ	CDR3β	%
1-2*01	23*01	CAVRDGSTQGGKLIF	13*01	1*01	2-1*01	CASSFPRNNEQFF	10.0
12-1*01	26*01	CVVNGRNYGQNFVF	4-1*01	2*01	2-7*01	CASSQPGGYEQSF	5.0
12-2*02	33*01	CAVNGLKDSNYQLIW	6-1*01	2*01	2-7*01	CASSEGGGYEQYF	5.0
17*01	37*02	CATHGSSNTGKLIF	7-3*01	-	2-7*01	CASSLFLAYEQYF	5.0
25*01	44*01	CAGKTGTASKLTF	27*01	2*02	2-7*01	CASSLGRLYEQYF	5.0
19*01	49*01	CALWCGNQFYF	27*01	1*01	2-1*01	CASGSNEQFF	5.0
3*01	3*01	CAVRDDYSSASKIIF	19*01	1*01	2-3*01	CASRDREDTQYF	5.0
10*01	43*01	CVVNPYNNNDMRF	9*01	2*02	2-7*01	CASSAGLAGAYEQYF	5.0
5*01	31*01	CAETSHNNARLMF	2*01	1*01	2-3*01	CASSESTGTDTQYF	5.0
13-1*02	11*01	CAPMNSGYSTLTF	7-9*01	1*01	2-6*01	CASSHLWVSGANVLTF	5.0
24*01	36*01	CARPGFRQTGANNLFF	3-1*01	1*01	2-1*01	CASSQDMDPYNEQFF	5.0
10*01	41*01	VVSGWSGYALIF	6-2*01	1*01	2-7*01	CASSYETGSSYEQYF	5.0
41*01	45*01	CASPGNSGGGADGLTF	25-1*01	1*01	2-6*01	CASTEGDVLTF	5.0
1-2*01	30*01	CAPTSDDKIIF	15*02	1*01	1-2*01	CATSPPGSGGYTF	5.0
12-2*02	35*01	CAVNHGLGGFGNVLHC	24-1*01	2*01	1-1*01	CATSVSGNTEAFF	5.0
14/DV4*02	33*01	CAMREGPMDSNYQLIW	7-9*01	1*01	1-6*01	CAVQGSYNSPLHF	5.0
3*01	37*01	VRCESQGGRSTGQLIF	30*01	1*01	2-5*01	CAWSVGRNGGETQYF	5.0
35*03	49*01	CAGQHGNQFYF	29-1*01	2*02	2-1*01	CSVEGTSGRSYNEQFF	5.0
8-2*03	8*01	CVVSDKGFQKLVF	2*01	2*02	2-2*01	VPSALLAGGPGSCF	5.0

VKU7

TRAV	TRAJ	CDR3α	TRBV	TRBD	TRBJ	CDR3β	%
13-2*01	11*01	CAEIALMNSGYSTLTF	2*01	1*01	2-7*01	CASSENRGYEQYF	4.0
12-1*02	33*01	CVVYGILDGNYQFTW	4-1*01	1*01	2-7*01	CASSRTGGYEQYF	4.0
2*01 F	37*01	CAAPLHSGNTGKLIF	6-6*01	1*01	2-7*01	CASSVGQGYEQYF	4.0
12-1*01	12*01	CVVNIMDSSYKLIF	2*01	1*01	2-7*01	CASSVSQGYEQYF	4.0
12-1*01	33*01	CVVNALRDSNYQLIW	6-1*01	1*01	2-7*01	CASSGGQGYEQYF	4.0
21*02	4*01	CGACHMFSGGYNKLIF	5-4*01	1*01	2-7*01	CASSLGVTYEQYF	4.0
6*02	49*01	CVIIPGTQFYF	2*01	1*01	2-7*01	CASRGQGGNEQYF	4.0
8-3*01	48*01	CAVRFNFGNEKLTF	9*01	1*01	1-1*01	CASSAPAGTEAFF	4.0
8-1*01	22*01	CLLLLRCGTRQLTF	6-6*01	1*01	2-5*01	CASSDATTQETQYF	4.0
8-4*01	31*01	CAVSETVNNARLMF	25-1*01	2*01	2-5*01	CASSEWGGQETQYF	4.0
3*01	15*01	CAVRERDQAGTALIF	9*01	2*01	2-5*01	CASSGTGGQETQYF	4.0
3*01	3*01	CAVRDPGYSSASKIIF	19*01	2*01	2-3*01	CASSIDLGDTQYF	4.0
14/DV4*02	53*01	CAMRPNSGGSNYKLTF	11-3*01	2*01	2-7*01	CASSLGVPGLSYEQYF	4.0
8-1*01	37*01	CAVNSGNTGKGIF	11-2*01	2*01	2-7*01	CASSLPGGQDYEQYF	4.0
17*01	23*01	CATDDNQGGKLIF	12-3*01	-	2-7*01	CASSLSYEQYF	4.0
3*01	29*01	CAVRDIIPGNTPLVF	7-9*03	2*02	2-7*01	CASSLTSGSPYEQYF	4.0
8-4*01	44*01	CAVRLYTGTASKLTF	14*02	2*02	1-4*01	CASSQGEVRNEKLFF	4.0
8-4*01	43*01	CAVSLNNNDMRF	5-4*01	1*01	2-7*01	CASSRTGQVNYEQYF	4.0
30*01	24*02	CGTTDSWGKLQF	7-3*01	1*01	2-3*01	CASSSGPADTQYF	4.0
9-2*01	52*01	CALSDNAGGTSYGKLTF	6-6*01	1*01	1-1*01	CASSYGSPNTEAFF	4.0
13-1*01	54*01	CAANPTQKLVF	7-9*03	2*02	2-1*01	CASSYPTSGSSYNEQFF	4.0
14/DV4*02	52*01	CAMRAGTSYGKLTF	6-5*01	2*02	2-7*01	CASSYSGAGVFYEQYF	4.0
8-4*01	32*02	CALDPPDPGGATNKLIF	20-1*01	2*01	2-1*01	CSARLAYSYNEQFF	4.0
9-2*03	6*01	CALSAASGGSYIPTF	20-1*01	2*02	2-1*01	CSASTSGRAVLFNEQFF	4.0
14/DV4*02	20*01	CAMRGTDDYKLSF	29-1*01	2*02	2-7*01	CSVQGTSGSFSYEQYF	4.0

VK10

TRAV	TRAJ	CDR3α	TRBV	TRBD	TRBJ	CDR3β	%
10*01	57*01	CVVSHLTQGGSEKLVF	2*01	2*02	2-7*01	CASSEGGRAYEQYF	33.3
21*02	39*01	CASFGAGNMLTF	11-3*04	2*01	2-7*01	CASSGTSGDEQYF	20.0
38-2/DV8*01	54*01	CAYRSAFWGAQKLVF	12-4*01	2*01	2-5*01	CASSFLAGPGETQYF	13.3
12-1*01	41*01	CVVNMLDSGYALNF	6-4*01	1*01	2-1*01	CASSEGQGYEQFF	6.7
8-4*01	47*02	CAVSVNGNKLVF	10-3*03	2*01	2-7*01	CAISENHGYEQYF	6.7
16*01	48*01	CALIGGNEKLTF	2*01	1*01	1-6*01	CASSPGTGRSPFHF	6.7
3*01	13*02	GLLNVSPGGYQKVTF	5-6*01	2*01	2-1*01	CASSPNSGEQFF	6.7
8-1*01	34*01	CALESYNTDKLIF	20-1*01	1*01	1-3*01	CSARVDIDGNTIYF	6.7

VK19

TRAV	TRAJ	CDR3α	TRBV	TRBD	TRBJ	CDR3β	%
12-3*01	44*01	CAFTGTASKLTF	7-8*01	2*02	2-1*01	CASSPELNEQFF	25.0
12-1*01	12*01	CVVNVPMDSSYKLIF	6-1*01	1*01	2-7*01	CASSEGTGYEQSF	8.3
12-1*01	12*01	CVVNMMDSSYKLIF	2*01	1*01	2-7*01	CASSESQGYEQYF	8.3
12-1*01	30*01	CVVNIRLDDKIIF	2*01	2*02	2-7*01	CASSEGGRAYEQYF	8.3
13-1*02	42*01	CAASMGYGGSQGNLIF	19*01	1*01	2-7*01	CASSMWLGYEQYF	8.3
8-1*01	31*01	CPAHNNARLMF	2*01	2*02	2-7*01	CASSENGGYEQYF	8.3
10*01	40*01	CVVSSLTTSGTYKYIF	7-6*01	1*01	2-7*01	CASSRTGAGEQYF	8.3
13-1*02	28*01	CAASAGSYQLTF	2*01	1*01	2-7*01	CASLGQETVDEQYF	8.3
26-1*01	48*01	CILHSSNFGNEKLTF	5-1*01	1*01	2-3*01	CASSGGQGLSTDTQYF	8.3
27*01	42*01	CAGADYGGSQGNLIF	2*01	2*01	2-2*01	CATRLARTGELFF	8.3

VK42

TRAV	TRAJ	CDR3α	TRBV	TRBD	TRBJ	CDR3β	%
26-1*01	52*01	CIVSPGTSYGKLTF	9*01	2*02	1-1*01	CASSAPVEGNTEAFF	17.6
12-1*01	18*01	CAVILGRGSTLGRLYF	5-1*01	1*01	1-2*01	CASSLEWADNYGYTF	11.8
8-6*02	41*01	CAVRRNSGYALNF	6-1*01	2*01	2-7*01	CASSESGGYEQYF	11.8
12-1*01	20*01	CAVNIPRSNDYKLSF	2*01	1*01	2-7*01	CASSENRGYEQYF	5.9
12-1*01	8*01	CVVADPALVF	2*01	1*01	2-7*01	CASSPWQNRVSSYEQYF	5.9
19*01	4*01	CALRGSGGYNKLIF	6-1*01	1*01	2-7*01	CASSDTGGYEQYF	5.9
2*01	33*01	CAVEDLNSNYQLIW	6-1*01	2*01	2-7*01	CASSEGLGYEQYF	5.9
4*01	5*01	CLVGDMDGDTGRRALTF	6-4*01	2*02	2-7*01	CASSEGVGYEQYF	5.9
34*01	47*02	CGADRYGNKLVF	5-6*01	1*01	1-1*01	CASSLGQGTEAFF	5.9
38-2/DV8*01	22*01	CAYLSPSGSARQLTF	10-3*01	2*01	2-5*01	CAISELGDPGGETQYF	5.9
21*01	31*01	CAVMELNARLMF	27*01	2*01	1-5*01	CASSLSRGQPQHF	5.9
12-2*02	4*01	CAVAGGYNKLIF	27*01	2*01	2-2*01	CASSPSSRNTGELFF	5.9
12-3*01	47*02	CAPYNNGNKLVF	4-1*01	1*01	2-5*01	CASSQGQGQETQYF	5.9

Supplemental Figure S2. TCR pairings of NF9 specific T-cells from <u>vaccinated</u> donors. Variable (V), joining (J), diversity (D) and CDR3 characteristics of NF9 specific TCR pairs. V-J genes colored according to circus plots used elsewhere in the study. The frequency of the TCR pairs are displayed. CDR3β motif CASSX^{3}GYEQYF, and motif-like CDR3s CASSX$^{2\text{-}8}$(G)YEQYF, are indicated.

GV38

TRAV	TRAJ	CDR3α	TRBV	TRBD	TRBJ	CDR3β	%
12-2*02	32*02	CAVELGGGATNKLIF	5-4*01	2*01	2-5*01	CASSPRGGQETQYF	6.9
13-1*02	12*01	CAASWSSYKLIF	12-4*01	1*01	2-3*01	CASSRPETGYDTQYF	6.9
12-1*01	28*01	CVVNILYSGAGSYQLTF	6-1*01	1*01	2-7*01	CASSEAKGYEQYF	3.4
12-1*01	28*01	CVVNAVAAGSYQLTF	5-4*01	1*01	2-7*01	CASSIGQGYEQYF	3.4
12-1*01	28*01	CVVILLSGAGSYQLTF	5-4*01	-	1-3*01	CASSLFMDTIYF	3.4
12-1*01	48*01	CVVTRISNFGNEKLTF	10-2*01	1*01	2-5*01	CASTKGWETQYF	3.4
12-3*01	18*01	CLALADRGSTLGRLYF	6-2*01	1*01	2-7*01	CASSTGQGYEQYF	3.4
39*01	53*01	CAVDGNSGGSNYKLTF	7-2*01	2*01	2-7*01	CASSLGLTGYEQYF	3.4
8-3*02	49*01	CAVGYSHLRITGNQFYF	6-4*01	2*02	2-7*01	CASSEAGGYEQYF	3.4
17*01	11*01	CATDSPGYSTLTF	4-3*01	1*01	1-2*01	CASHKFRGANYGYTF	3.4
17*01	54*01	CATDVRTQKLVF	2*01	2*01	2-7*01	CASRPWGTSDYEQYF	3.4
14/DV4*01	40*01	CAMSRSGTYKYIF	9*01	1*01	2-3*01	CASSAPRGGQSTDTQYF	3.4
8-3*02	53*01	CAVDPNSGGSNYKLTF	11-3*04	2*01	2-1*01	CASSDLAGSNEQFF	3.4
14/DV4*01	30*01	CAMRELRDDKIIF	25-1*01	1*01	1-2*01	CASSESYTVYGYTF	3.4
21*01	49*01	CAVEANTGNQFYF	6-2*01	-	2-7*01	CASSHAYEQYF	3.4
19*01	3*01	CARAYSSASKIIF	13*01	1*01	2-1*01	CASSLRDSYNEQFF	3.4
17*01	42*01	CATFYGGSQGNLIF	27*01	1*01	1-2*01	CASSLSDRGAYGYTF	3.4
1-1*01	40*01	CAARTTSGTYKYIF	19*01	2*01	1-2*01	CASSMEGGQFPYGYTF	3.4
12-3*01	5*01	CATNSMDTGRRALTF	6-5*01	1*01	2-3*01	CASSPWTGNTDTQYF	3.4
13-1*02	17*01	CAASMEAAGNKLTF	4-1*01	2*01	2-1*01	CASSQEGLANNEQFF	3.4
8-1*02	16*02	FRAPCSCKDDHKLMF	4-1*01	1*01	2-2*01	CASSQGVVLQGELFF	3.4
13-2*01	52*01	CAESPNAGGTRYGKLTF	4-1*01	2*02	2-1*01	CASSQWSGSNYEQFF	3.4
8-1*01	39*01	CAVTLLNAGNMLTF	5-5*02	1*01	2-7*01	CASSRTQYYEQYF	3.4
12-2*02	28*01	CAVMSYSGAGSYQLTF	9*01	2*01	2-7*01	CASSVASGAYEQYF	3.4
27*01	38*01	CAGPHAGNNRKLIW	6-6*01	1*01	1-5*01	CASSYLGGPSNQPQHF	3.4
14/DV4*02	24*03	CAMREREATDSWGKFQF	30*01	1*01	1-4*01	CAWSPGFPPNEKLFF	3.4
13-1*02	8*01	CAASRVDTGFQKLVF	20-1*01	2*01	2-3*01	CSARSPIVTDTQYF	3.4

GV41

TRAV	TRAJ	CDR3α	TRBV	TRBD	TRBJ	CDR3β	%
12-1*01	6*01	CVVNGWEGGSYIPTF	20-1*01	2*01	2-3*01	CSARDRQADDTDTQYF	5.6
21*01	18*01	CAVRSDRGSTLGRLYF	11-2*03	1*01	2-7*01	CASSLGQGYEQYF	5.6
14/DV4*02	11*01	CAFPFSGYSTLTF	27*01	1*01	2-7*01	CASSLWQGYEQYF	5.6
12-2*01	42*01	CAVLNYGGSQGNLIF	10-3*03	2*01	2-7*01	CAISEGRAYEQYF	5.6
4*01	42*01	CLVIYGGSQGNLIF	4-1*01	2*02	2-7*01	CASSQGESYEQYF	5.6
4*01	22*01	CLVWGSARQLTF	2*01	1*01	2-7*01	CASSEGTGGYEQYF	5.6
4*01	10*01	CLVGDMNRFTGGGNKLTF	5-6*01	1*01	2-7*01	CASSLGGRGYEQYF	5.6
3*01	47*02	CAVRDDSYGNKLVF	5-6*01	2*02	2-3*01	CASSLEVGKWTDTQYF	5.6
8-6*01	4*01	CATSGGYNKLIF	28*01	1*01	1-1*01	CASSPRTGWTEAFF	5.6
17*01	15*01	CATGLNQAGTALIF	29-1*01	2*02	1-3*01	CSVEVTAPGEGGNTIYF	5.6
38-2/DV8*01	41*01	QAYRSTGYAETL	29-1*01	1*01	2-7*01	CSVVGVRPDEQYF	5.6
19*01	29*01	CALSESNSGNTPLVF	24-1*01	1*01	2-7*01	CATSAVGHSGNEQYF	5.6
3*01	23*01	CAVRFPGNQGGKLIF	28*01	2*01	2-1*01	CASRPGLAGDNEQFF	5.6
21*01	44*01	PQAGTASKLTF	20-1*01	1*01	2-7*01	CSASRLGTGSYEQYF	5.6
8-3*02	41*01	CAVGLSGYALNF	19*01	1*01	2-7*01	CASSIERRTSDYEQYF	5.6
6*02	43*01	CALDNNNNDMRF	28*01	2*01	2-7*01	CASRLRDWDDEQYF	5.6
4*01	5*01	CLVGDTRPQDTGRRALTF	4-2*01	2*01	2-3*01	CASSQGSGGDTQYF	5.6
29/DV5*04	20*01	CAARLSNDYKLSF	4-1*01	1*01	2-1*01	CASWDANRNEQFF	5.6

KK-008

TRAV	TRAJ	CDR3α	TRBV	TRBD	TRBJ	CDR3β	%
12-1*01	41*01	CVVNMLRNSGYALNF	6-1*01	2*01	2-7*01	CASSESGGYEQYF	22.5
26-1*02	23*01	CIGAYNQGGKLIF	2*01	2*01	2-7*01	CASSENRGYEQYF	9.8
12-1*01	12*01	CVVNIIMDSSYKLIF	6-4*01	2*02	2-7*01	CASSEGEGYEQYF	8.8
12-1*01	33*01	CVVNEYRSSNYQLIW	5-4*01	1*01	2-7*01	CASSLGQGYEQYF	8.8
12-1*01	12*01	CVVNLMDSSYKLIF	2*01	1*01	2-7*01	CASSVSQGYEQYF	6.9
1-1*01	30*01	CAVRGKNRDDKIIF	20-1*01	1*01	2-3*01	CSARPRDWGLGTDTQYF	5.9
12-1*01	12*01	CVVNMLLDSSYKLIF	4-1*01	1*01	2-1*01	CASSDTQGYEQFF	4.9
12-1*01	54*01	CVVNTPIQGAQKLVF	2*01	1*01	2-7*01	CASSENRKDPNSC	4.9
12-1*01	33*01	CVVIIRGDSNHQLTW	7-3*01	1*01	2-7*01	CASSYGQGYEQYF	3.9
12-1*01	28*01	CVVNRLGAGSYQLTF	7-2*02	1*01	2-7*01	CASSSGQGYEQYF	3.9
38-1*01	40*01	CAFFLEGTYKYIF	20-1*01	2*02	2-7*01	CSVGASGSYEQYF	3.9
12-1*01	12*01	CVVNRMDSSYKLIF	10-3*03	1*01	2-7*01	CAISEQQGYEQYF	3.9
24*01	53*01	CAFPVGGSNYKLTF	20-1*01	2*01	2-7*01	CSARDISGGGQYEQYF	3.9
26-1*02	37*02	CIVMGSSNTGKLIF	2*01	1*01	2-7*01	CASSEFRTYEQYF	2.9
12-1*01	28*01	CVVNIHSGAGSYQLTF	5-4*01	1*01	2-7*01	CASSIGQGYEQYF	2.0
12-1*01	28*01	CVVNKHSGAGSYQLTF	5-4*01	1*01	2-7*01	CASSQGQGYEQYF	2.0
20*02	57*01	CVRYLTPQGGSEKLVF	2*01	1*01	2-7*01	CASSEFQGYEQYF	1.0

GV42

TRAV	TRAJ	CDR3α	TRBV	TRBD	TRBJ	CDR3β	%
5*01	24*02	CAEVVNDSWGKLQF	2*01	1*01	2-7*01	CASSESQGYEQYF	4.9
19*01	7*01	CALSEATGGGNNRLAF	5-5*02	1*01	1-5*01	CASSLGWGNQPQHF	3.3
12-1*01	9*01	CVVNMWGTGDFKIIF	27*01	1*01	2-1*01	CASGALGNEQFF	3.3
12-1*01	12*01	CVVNLLMDSSYKLIF	2*01	1*01	2-4*01	CASSEGQGYIQYF	1.6
12-1*01	43*01	CVVTPVPNDMRF	6-1*01	1*01	2-7*01	CASSEGQSYEQYF	1.6
12-1*01	12*01	CVVNALEDSSYKLIF	2*01	1*01	2-7*01	CASSAGQGYEQYF	1.6
12-1*01	12*01	CVVNIFLDSSYKLIF	2*01	2*01	2-7*01	CASSATAGYEQYF	1.6
12-1*01	40*01	CVVSPPGPSGTYKYIF	2*01	1*01	2-7*01	CASSDFQGYEQYF	1.6
12-1*01	42*01	CVVTPNYGGSQGNLIL	2*01	1*01	2-7*01	CASSEYMSYEQYF	1.6
12-1*01	34*01	CVVQGDTDKLIF	6-1*01	1*01	2-7*01	CASSDWVGYEQYF	1.6
12-2*01	53*01	CAVNGLAGGSNYKLTF	6-1*01	1*01	2-7*01	CASSEGSGYEQYF	1.6
12-1*01	12*01	CVVNRLMDSSYKLIF	6-1*01	2*01	2-7*01	CASSVAKGYEQYF	1.6
12-2*01	28*01	CASSRPSSGAGSYQLTF	6-1*01	1*01	2-7*01	CASSEWGQGYEQYF	1.6
12-1*01	20*01	CVVSGDYKLSF	2*01	2*01	2-7*01	CASSEFAGKGSSYEQYF	1.6
12-1*01	5*01	CVVNIGTGRRALTF	4-1*01	1*01	2-7*01	CASSLGQDYEQYF	1.6
12-1*01	12*01	CVVTRWMDSSYKLIF	5-6*01	2*01	2-1*01	CASSHWTLQPDNEQFF	1.6
12-1*01	8*01	CVVNGRWNANTGFQKLVF	9*01	2*01	2-7*01	CASSVAWTSVYEQYF	1.6
38-2/DV8*01	39*01	CAYHNNAGNMLTF	11-2*01	1*01	2-7*01	CASSRWQNYEQYF	1.6
20*02	10*01	CAVQTGGGNKLTF	6-4*01	2*01	1-2*01	CASSDGLGYTF	1.6
34*01	21*01	CGAASPGGKFYF	2*01	1*01	2-7*01	CASSEYTPLGHEQYF	1.6
8-3*01	42*01	CAVGIYGGSQGNLIF	12-4*01	2*01	2-1*01	CASSFGSGAYNEQFF	1.6
4*01	43*01	CLVGDSDDMRF	7-9*03	1*01	1-1*01	CASSFRGTEAFF	1.6
16*01	49*01	CALTSGNQFYF	4-2*01	2*02	2-7*01	CASSHMSSGNYEQYF	1.6
8-4*01	22*01	CAVSDVYGSARQLTF	19*01	2*01	2-3*01	CASSIGGRTTDTQYF	1.6
38-1*03	36*01	CAFIGLTGANNLFF	19*01	2*02	2-5*01	CASSILSGRTGGETQYF	1.6
8-3*01	47*01	CAVVPMEYGNKLVF	7-9*03	1*01	2-3*01	CASSLALRQGATDTQYF	1.6
41*01	32*02	CAVRPGYGGATNKLIF	5-4*01	2*01	2-3*01	CASSLALTDTQYF	1.6
24*01	6*01	CASRRLSGGSYIPTF	2*01	1*01	2-3*01	CASSLDWGTAHTDTQYF	1.6
14/DV4*01	39*01	CSMIEDNTDTMLTF	7-9*03	2*02	1-1*01	CASSLGGGKVNTEAFF	1.6
9-2*04	49*01	CAPPNTGNQFYF	13*01	1*01	2-6*01	CASSLGQGQGYSGANVLTF	1.6
16*01	10*01	CARRGGNKLTF	7-3*01	1*01	2-3*01	CASSLSGGGTDTQYF	1.6
8-6*02	9*01	CAVDTGGFKTIF	7-9*03	1*01	1-2*01	CASSLTRTLPKGQLYGYTF	1.6
20*02	39*01	CAVPNNNAGNMLTF	4-1*01	2*02	2-7*01	CASSQDFSGSYEQYF	1.6
8-1*01	5*01	CAVFPWAGRRALTF	14*01	2*02	1-1*01	CASSQGGGDTEAFF	1.6
12-3*01	34*01	CAMSHYNTDKLIF	5-1*01	-	2-5*01	CASSSEETQYF	1.6
21*02	18*01	CAVQGRGSTLGRLYF	9*01	1*01	2-5*01	CASSSEGGVGETQYF	1.6
8-4*03	49*01	CAVTFSNQFYF	7-9*03	2*01	1-1*01	CASSSRGATGTEAFF	1.6
22*01	12*01	CAVWMDSSYKLIF	9*01	1*01	1-1*01	CASSVAGVTEAFF	1.6
12-2*02	35*01	CAVNMPPIGFGNVLHC	9*01	2*01	2-1*01	CASSVGPGVGNEQFF	1.6
14/DV4*02	42*01	CALVRYYGGSQGNLIF	6-4*01	2*02	2-1*01	CASSVSGSEGHEQFF	1.6
29/DV5*04	43*01	CAATWGDMRF	5-1*01	2*01	2-3*01	CASSYWGGSDTQYF	1.6
13-1*02	21*01	CAAGSTLYNFNKFYF	4-1*01	1*01	1-1*01	CASTGRAGGTEAFF	1.6
13-1*02	43*01	CAASMRDNDMRF	15*02	1*01	2-7*01	CATSKESGAPYEQYF	1.6
3*01	49*01	CAVRDTGNQFYF	30*01	1*01	1-2*01	CAWNHGGLYGYTF	1.6
5*01	40*01	CAVTSGTYKYIF	30*01	1*01	2-1*01	CAWSPLKGREQFF	1.6
12-3*01	53*01	CAIGGSNYKLTF	20-1*01	2*02	2-1*01	CSAHGGPTSGSFIEQFF	1.6
8-4*01	10*01	CAVTLHGGGNKLTF	20-1*01	2*02	2-3*01	CSAPTEERTDTQYF	1.6
22*01	20*01	CAVERKQTSSAF	20-1*01	1*01	2-1*01	CSARAGETFSSYNEQFF	1.6
19*01	13*02	CALSERNSGGYQKVTF	20-1*01	1*01	2-3*01	CSARARQDHTDTQYF	1.6
38-2/DV8*01	30*01	CAYRSARDDKIIF	20-1*01	1*01	2-7*01	CSAREQDYEQYF	1.6
13-2*01	39*01	CAENSYNNAGNMLTF	20-1*01	2*01	2-1*01	CSARPLAASSYNEQFF	1.6
12-2*01	45*01	CAVNIGSGGGADGLTF	29-1*01	1*01	2-3*01	CSAWDRFTDTQYF	1.6
38-1*03	39*01	CAFMKPNAGNMLTF	20-1*01	1*01	1-3*01	CSGMDGSSGNTIYF	1.6
19*01	41*01	CALSTSNSGYALNF	29-1*01	2*02	2-1*01	CSVEGLAGEWEQFF	1.6
17*01	3*01	CATHLRGSSASKIIF	29-1*01	2*01	2-5*01	CSVVLAENAEETQYF	1.6
12-2*01	53*01	CAVNDSGGSNYKLTF	20-1*01	1*01	2-7*01	CSSVSISSYEQYF	1.6
4*01	9*01	CLTPYTGGFKTIF	28*01	1*01	1-6*01	CASIPYQDRGLFEMNSPLHF	1.6

Supplemental Figure S3. TCR pairings of NF9 specific T-cells from <u>convalescent</u> donors. Variable (V), joining (J), diversity (D) and CDR3 characteristics of NF9 specific TCR pairs. V-J genes colored according to circus plots used elsewhere in the study. The frequency of the TCR pairs are displayed. CDR3β motif CASSX^{3}GYEQYF, and motif-like CDR3s CASSX$^{2\text{-}8}$(G)YEQYF, are indicated.

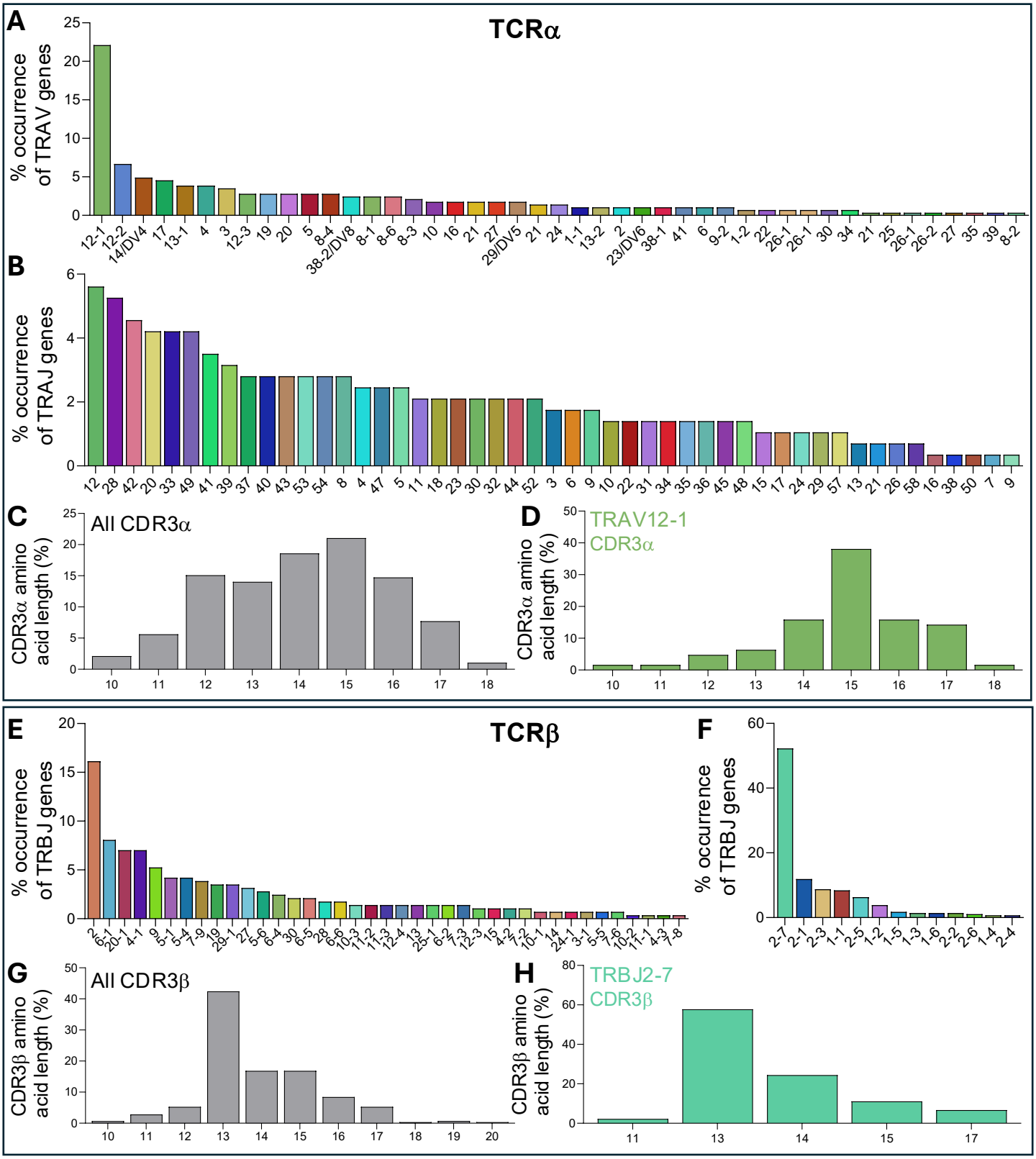

Supplemental Figure S4. TCRα and TCRβ characteristics of NF9-specific T-cell responses in vaccinated and convalescent donors. (**A**) TCRα V-gene usage. (**B**) TCRα J-gene usage. (**C**) CDR3α length. (**D**) CDR3α length of TRAV12-1 containing CDR3α. (**E**) TCRβ V-gene usage. (**F**) TCRβ J-gene usage. (**G**) CDR3β length. (**H**) CDR3β length of TRBJ2-7 containing CDR3α.

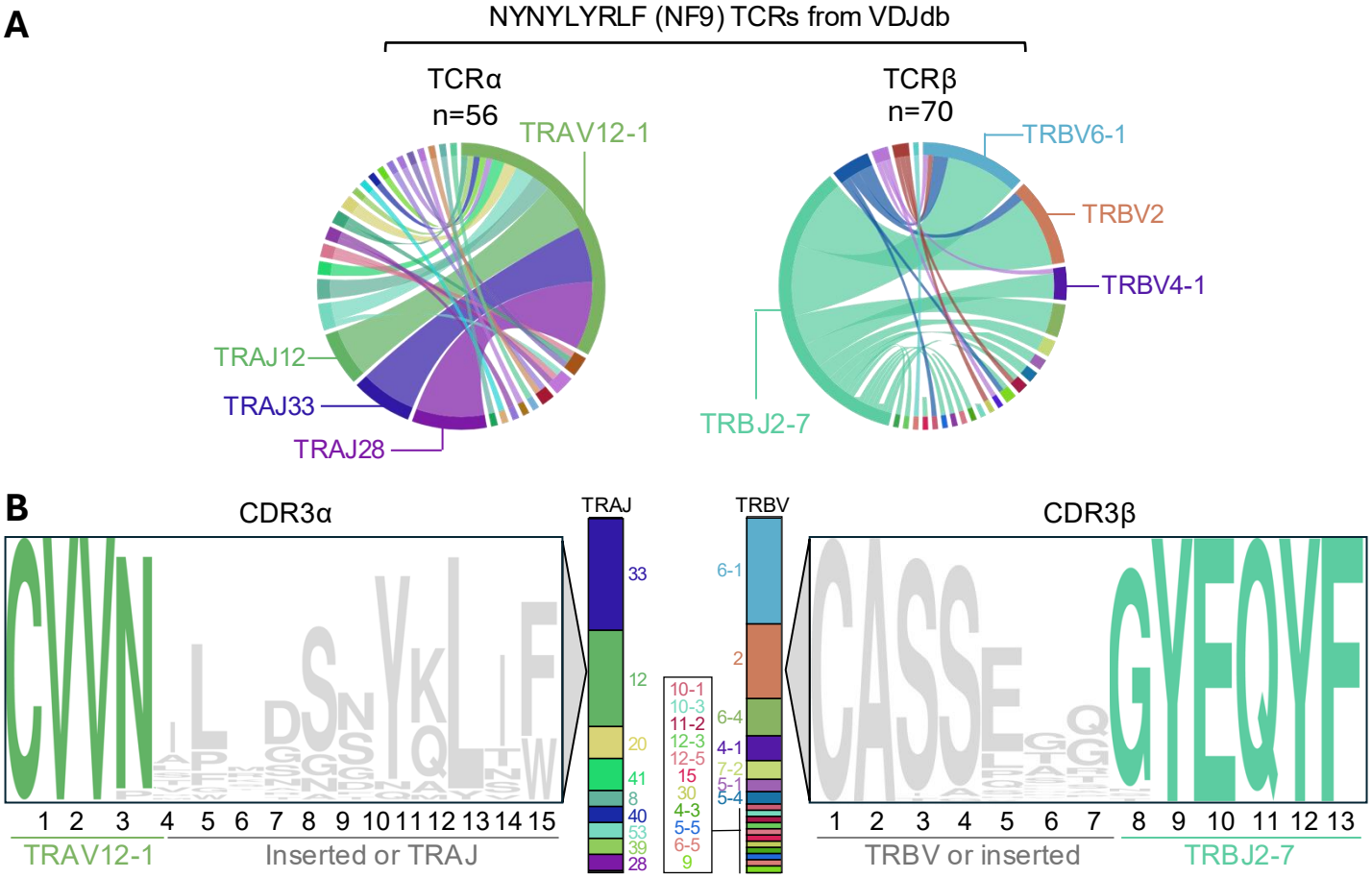

Supplemental Figure S5. Clonotypic analysis of NYNYLYRLF-containing CDR3 sequences from VDJdb. Data taken from VDJdb for HLA-A*24:02 NYNYLYRLF specific TCRs including CDR3s with TRAV-TRAJ (56 chains) and TRBV-TRBJ (70 chains) gene usage. (**A**) Circos plots show the proportion of TRAJ or TRBJ genes on the left and TRAV or TRBV genes on the right, with the size of the arcs corresponding to relative frequency of the genes. Ribbons between the arcs represents V-J pairings. (**B**) Logo plots of CDR3α (left) and CDR3β (right) from VDJdb TCRs in (**A**). CDR3α: based on TRAV12-1 (most prevalent TRAV) of 15 amino acids in length. CDR3β motif: based on TRBJ2-7 and 13 amino acids in length. The multiple TRAJ and TRBV chains that contribute to the CDR3 motifs are shown in central bars, where they are ordered from highest to lowest frequency.

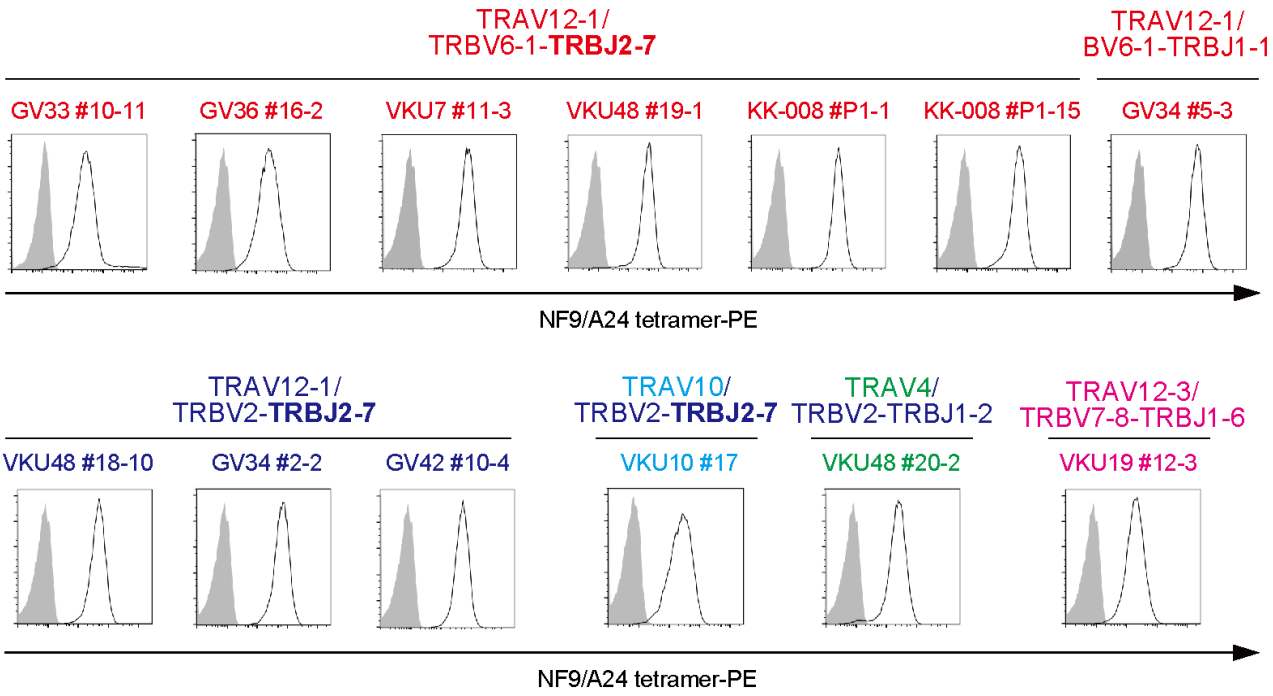

Supplemental Figure S6. A24/NF9 tetramer staining of TCR-transduced Jurkat cells. A Jurkat cells alone (shaded histogram) or those expressing A24/NF9-specific TCRs (GV33 #10-11, GV34 #5-3, GV36 #16-2, VKU7 #11-3, VKU48 #19-1, KK-008 #P1-1, and KK-008 #P1-15, VKU48 #18-10, GV34 #2-2, GV42 #10-4, VKU #20-2, VKU #17 and VKU #12-3) (open histogram) were stained with anti-CD3 mAb and A24/NF9 tetramer and then analyzed by flow cytometry.

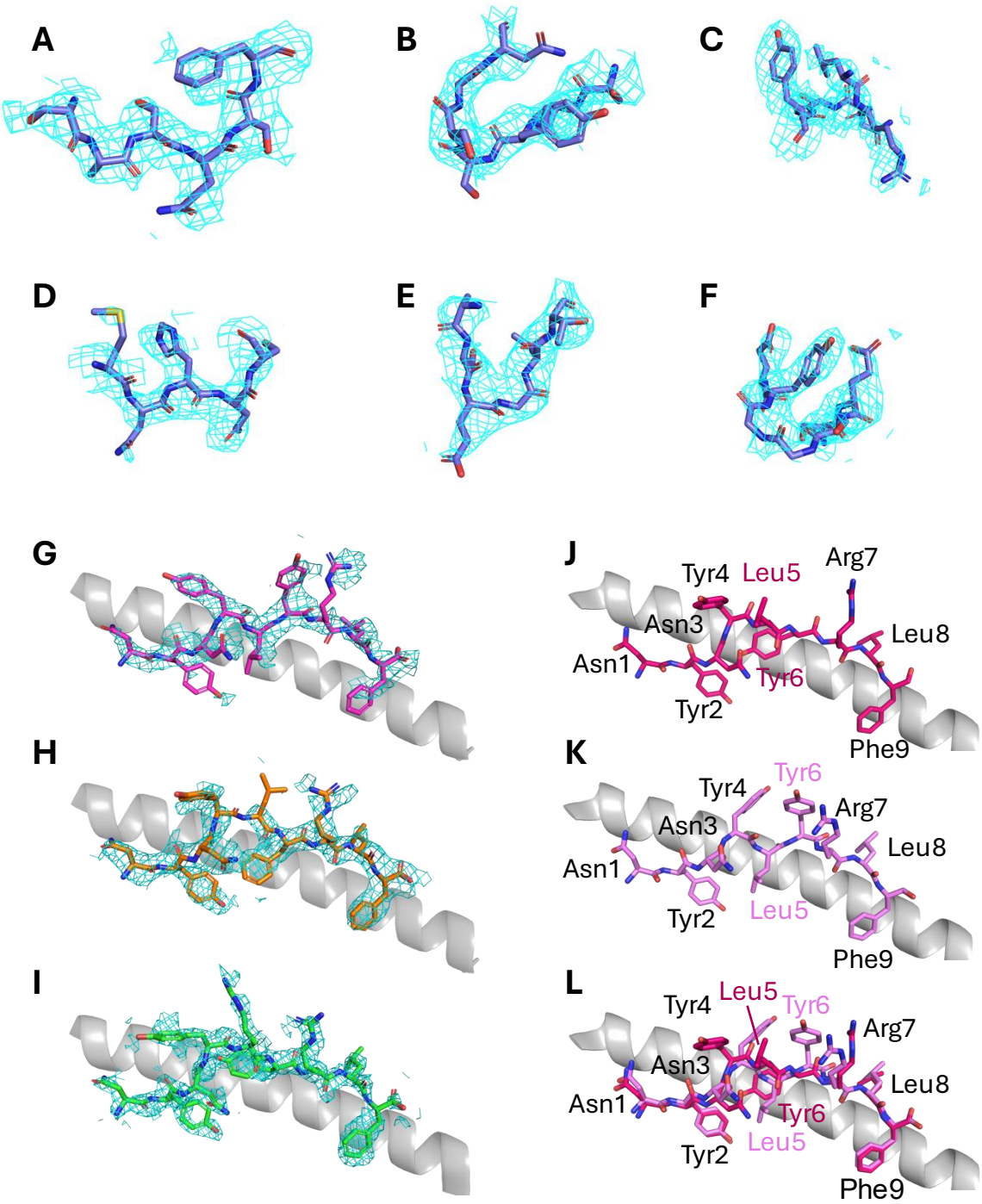

Supplemental Figure S7. OMIT maps confirming robustness of X-ray crystallography models and Conformational change of the NF9 peptide and TCR cross-reactivity (A-F) 3D structural maps of P1-15 Complementary Determining Regions (CDR) Loops (**A** – CDR1α, **B** – CDR2α, **C** – CDR3α, **D** – CDR1β, **E** – CDR2β, **F** – CDR3β) accompanied by their respective electron densities (cyan mesh). Unbiased omit maps were calculated after removal of the loops from the model to minimise model bias. (**G–I**) 3D structural maps of the NF9 peptide in complex with the P1-15 TCR (magenta sticks), NF9-6F peptide (orange sticks), and NF9-5R peptide (green sticks), accompanied by their respective electron densities (cyan mesh). Unbiased omit maps were calculated after removal of the peptide from the model to minimise model bias. The resulting electron density supports the assigned peptide backbone conformations and clearly resolves the distinct P5 and P6 orientations described in the main text. (**J**) Presentation of copy 1 of the NF9 peptide when not in complex with TCR, published by Zhang et al. (PDB 7F4W). (**K**) As in (A) but copy 2 published by Zhang et al. (PDB 7F4W). (**L**) Comparison of copy 1 and 2 from (A) and (B).

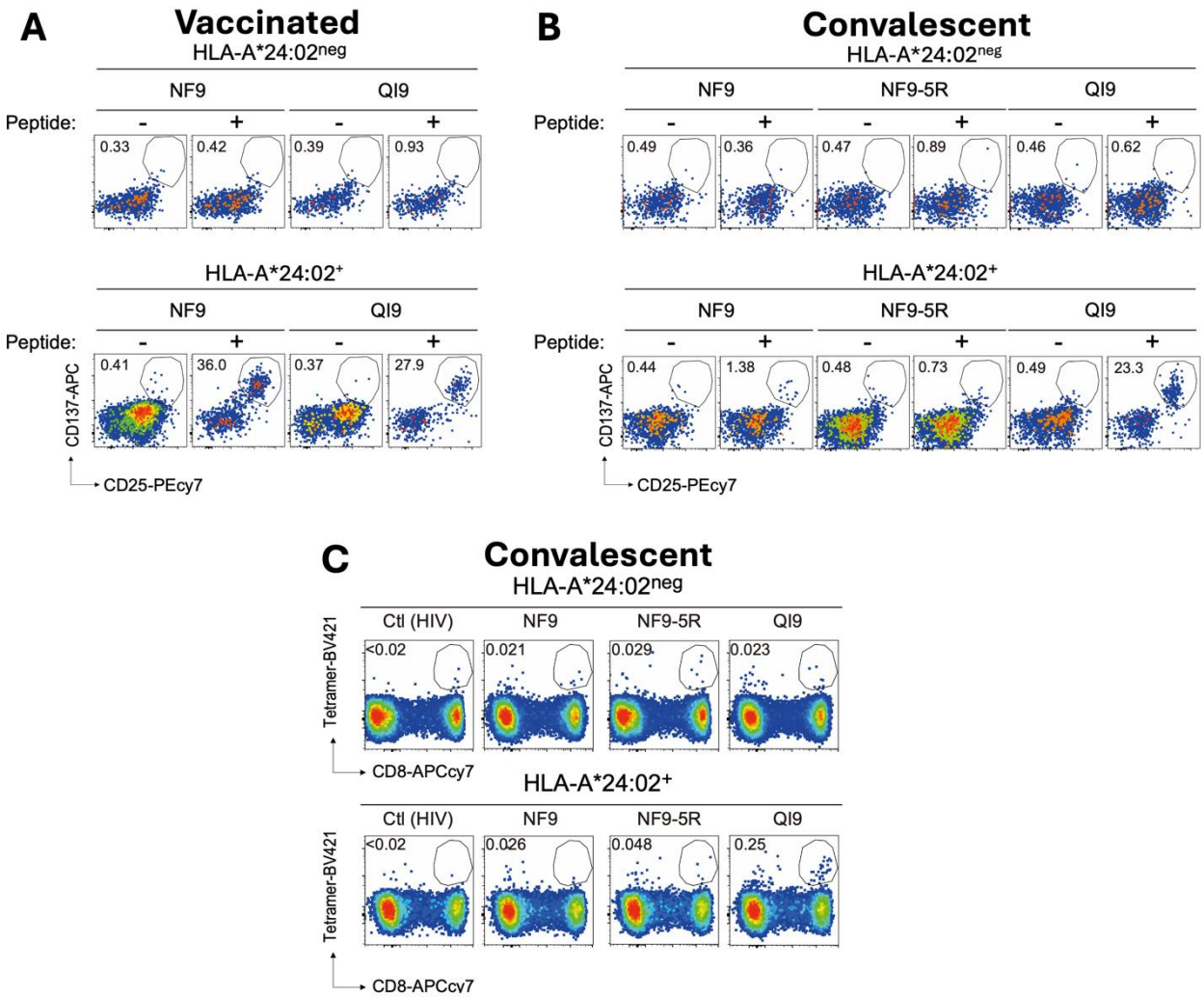

Supplemental Figure S8. NF9 5R specific T-cells are not detectable in convalescent donors infected with the SARS-CoV-2 Delta variant: example flow cytometry plots. (**A**) PBMCs from vaccinated donors stimulated with NF9 and QI9 peptides. Example flow cytometry plots shown for an HLA-A*24:02^{neg} or HLA-A*24:02^{+} donor. (**B**) PBMCs from convalescent donors infected with the delta strain. Example flow cytometry plots shown for an HLA-A*24:02^{neg} or HLA-A*24:02^{+} donor. (**C**) Tetramer staining of PBMCs from HLA-A*24:02 negative (n = 6) or positive (n = 8) convalescent donors infected with the delta strain. Example flow cytometry plots shown for an HLA-A*24:02^{neg} or HLA-A*24:02^{+} donor.